Received 14 January 2022; revised 1 March 2022; accepted 2 March 2022. Date of publication 24 March 2022; date of current version 4 April 2022.

Digital Object Identifier 10.1109/OJAP.2022.3162110

Next-Generation Healthcare: Enabling Technologies for Emerging Bioelectromagnetics Applications

ASIMINA KIOURTI[1] (Senior Member, IEEE), AMIN M. ABBOSH[2] (Fellow, IEEE), MARIA ATHANASIOU[3] (Student Member, IEEE), TONI BJÖRNINEN[4] (Senior Member, IEEE), ALINE EID[5] (Graduate Student Member, IEEE), CYNTHIA FURSE[6] (Fellow, IEEE), KOICHI ITO[7] (Life Fellow, IEEE), GIANLUCA LAZZI[8] (Fellow, IEEE), MOHAMED MANOUFALI[2] (Member, IEEE), MATTEO PASTORINO[9] (Fellow, IEEE), MANOS M. TENTZERIS[5] (Fellow, IEEE), KATRINA TISDALE[1] (Graduate Student Member, IEEE), ERDEM TOPSAKAL[10] (Senior Member, IEEE), LEENA UKKONEN[11] (Member, IEEE), WILLIAM G. WHITTOW[12] (Senior Member, IEEE), HUANAN ZHANG[13], AND KONSTANTINA S. NIKITA[3] (Fellow, IEEE)

[1]Department of Electrical and Computer Engineering, Ohio State University, Columbus, OH 43212, USA

[2]School of Information Technology and Electrical Engineering, University of Queensland, Brisbane, QLD 4072, Australia

[3]School of Electrical and Computer Engineering, National Technical University of Athens, 15780 Athens, Greece

[4]Faculty of Information Technology and Communication Sciences, Tampere University, 33014 Tampere, Finland

[5]School of Electrical and Computer Engineering, Georgia Institute of Technology, Atlanta, GA 30332, USA

[6]Department of Electrical and Computer Engineering, University of Utah, Salt Lake City, UT 84112, USA

[7]Center for Frontier Medical Engineering, Chiba University, Chiba 263-8522, Japan

[8]Viterbi School of Engineering, University of Southern California, Los Angeles, CA 90089, USA

[9]Department of Electrical, Electronic, Telecommunications Engineering and Naval Architecture, University of Genoa, 16145 Genoa, Italy

[10]Department of Electrical and Computer Engineering, Virginia Commonwealth University, Richmond, VA 23284, USA

[11]Faculty of Medicine and Health Technology, Tampere University, 33014 Tampere, Finland

[12]School of Mechanical, Electrical and Manufacturing Engineering, Loughborough University, Loughborough LE11 3TU, U.K.

[13]Department of Chemical Engineering, University of Utah, Salt Lake City, UT 84112, USA

CORRESPONDING AUTHOR: K. S. NIKITA (e-mail: knikita@ece.ntua.gr)

ABSTRACT Rapid advances in antennas, propagation, electromagnetics, and materials are opening new and unexplored opportunities in body area sensing and stimulation. Next-generation wearables and implants are seamlessly providing round-the-clock monitoring. In turn, numerous applications are brought forward with the potential to ultimately transform healthcare, sports, consumer electronics, and beyond. This review paper provides a comprehensive overview, discusses challenges and opportunities, and indicates future directions for: (a) enabling technologies needed to make body area sensing and stimulation a reality, and (b) emerging bioelectromagnetics applications that may readily benefit from such technologies.

INDEX TERMS Implants, wearables, wireless power transfer, wireless telemetry, neurosensing, neurostimulation, materials, microwave imaging, electromagnetic imaging, bioelectromagnetics, dosimetry.

I. INTRODUCTION

RAPID advances in mobile, wireless, and sensing technologies are opening up new opportunities in body area sensing and stimulation, promising an entirely new realm of applications in healthcare, sports, gaming, consumer electronics, and beyond [1]. Remote diagnosis, patient and elderly monitoring, sensing of vital parameters of people suffering from chronic diseases such as asthma, diabetes,

neurodegenerative and cardiovascular diseases, are just a few examples.

The development of such transformative applications entails critical requirements and challenges, including timely and reliable access to diagnostic information, energy-efficient biosensor design, biocompatibility, system integration, sensor miniaturization, patient safety, emergency response, and detection. Groundbreaking technological developments in antennas, electromagnetics, and materials can address these challenges and revolutionize healthcare delivery and wellness management. This can be enabled through next-generation implants and wearables that, in turn, enable emerging bioelectromagnetics applications such as neurosensing, neurostimulation, and innovative imaging modalities [2]. Indeed, disease detection and diagnosis using wireless medical devices is seen as a transformative approach to healthcare, addressing the unsustainability of current healthcare provision models.

Wireless implants are integrated with efficient implantable antennas, which, depending on the application, may operate in subcutaneous and/or deep-tissue environments [3]–[5]. Wireless capabilities permit unobtrusive and ubiquitous communication with exterior monitoring/control equipment, such as a smart phone, smart watch, or other type of smart wearable garment. Accordingly, the design of wearable antennas has attracted significant scientific interest for reducing absorption by the lossy biological tissues, optimizing radiation efficiency, miniaturizing their footprint, and so on [6]. In other cases, particularly when the distance between the transmitter and receiver is short, wireless telemetry may be performed via inductive links [7]. Optimized single- and multi-coil configurations have long been reported in this regard.

Additionally, the science of wirelessly powering medical devices becomes increasingly relevant and significant. For wearables, wireless powering may be a matter of convenience, but, for implants, wireless powering further enhances patient safety and minimizes healthcare costs. That is, Wireless Power Transfer (WPT) makes biomedical implants more practical thanks to the appeal of charging wirelessly and conveniently [8]. Electromagnetic-based wireless powering solutions range from inductive to Radio-Frequency (RF) links, both of which are viewed as critical enabling components. Assuming a wireless implant, inductive powering entails implanted and on-body coils that transfer energy by means of magnetic flux and Faraday's law. In the case of wireless RF powering (namely, RF power harvesting), antennas are used to capture the abundant electromagnetic energy radiated by random or dedicated sources in the surrounding environment.

Advances in materials and related fabrication techniques are also critical towards the development of seamless implants and wearables. Flexible materials along with additive manufacturing technologies like inkjet printing have brought forward the development of conformal, flexible and robust antennas and electronics for use with everyday clothing, wearable sensors, biomedical wireless sensors and radio frequency identification (RFID) systems [9]–[11]. Biocompatible, biostable, and soft materials that do not compromise conductivity are also emerging, promising safe chronic *in vivo* performance of wireless implants [12].

Once the prototype is assembled, evaluation of in tissue-emulating phantoms circumvents numerous limitations associated with conventional *in vivo* testing. A multitude of recipes has been reported in this regard, including phantoms of diverse consistencies, emulating diverse types of tissues across diverse frequencies and bandwidths [13], [14]. Dosimetry studies are of paramount importance at this evaluation stage as well, helping to ensure patient safety via conformance with national and/or international standards for the specific absorption rate (SAR) [15].

Overall, wireless medical devices used to sense physiological parameters (sensors) and stimulate the nervous system (stimulators) are becoming increasingly vital and can facilitate medical prevention, diagnosis, and treatment of a multitude of conditions including cancer, chronic pain, and neurological disorders. Image-guided Microwave Ablation (MWA) has emerged as a minimally invasive therapeutic modality for the treatment of unresectable tumors and cardiac arrhythmias, neuromodulation, and other applications [16]. Antennas used in MWA systems should ensure efficient power transfer to tissue, through a heating pattern well matched to the size and shape of the targeted tissue. Furthermore, microwave techniques have gained increased research interest towards the development of Microwave Imaging (MWI) systems, due to reduced complexity and miniaturization advantages compared to other techniques. Clinical applications of MWI include breast cancer screening, monitoring of fluid accumulation in the lungs, triaging of stroke patients, and more. The advent of wearable electromagnetic systems has further pushed research towards this direction, sparking the intensive study of flexible and bio-matched radiating devices to be employed in portable systems [17]. Deep brain neurosensors and neurostimulators have recently attracted significant interest for several applications, including epilepsy, Parkinson's disease, Alzheimer's disease, addictions, etc. Wireless and batteryless brain implants are envisioned to enable continuous monitoring of neural activity with minimum impact on the individual's activity [18]. Furthermore, implantable neurostimulators [19] constitute a promising solution and are used to stimulate the nervous system in order to treat and relieve symptoms of visual impairment, Parkinson's, dystonia, depression, Alzheimer's, sleep apnea, chronic pain, and many more. Within this framework, several research efforts are pursued in order to address challenges related to electrode shape and size, miniaturization and biocompatibility issues, microantenna design enabling high-data rate transmission, etc.

II. ENABLING TECHNOLOGIES

A. WIRELESS TELEMETRY

1) RF TELEMETRY

1) Wearable Antennas: Wearable antennas have gained popularity in recent years due to increased number of Internet of

TABLE 1. Some of the most highly cited journal papers about wearable antennas.

Ref. Year	Antenna description	Fabrication technology	Freq (GHz)	Key points
[22] 2009	CPW monopole above 3×3 EBG	Felt & Zelt conducting nylon	2.45 and 5	3 x 3 EBG was effective in reducing SAR. Bending in E plane affects performance more than in H plane. Gain was increased compared to patch antenna.
[23] 2006	CP patch antenna	Various nickel-plated fabric sheets	2.4	Antenna can withstand bends on radius of 37.5 mm. Harder to maintain CP when bent.
[24] 2009	CP patch antenna	4 mm thick shock absorbing foam; Shieldit Super for the conductor	2.4	FlecTron was used for the ground plane because it can be soldered onto. Paper investigates compressing. the foam and bending. The structure was waterproofed.
[25] 2015	NFC RFID Tag	Circuitry is solder-reflow-integrated on a standard Cu/polyimide flexible-electronic layer	13.56	Integrated with sweat sensor. Feels like a sticking plaster. Has been demonstrated to work for 7 days.
[26] 2013	M-shaped monopole over Jerusalem Cross AMC	A silver nano particle conductive ink was printed on flexible Kapton polyimide substrate	2.45	The AMC increases the front to back ratio by 8 dB and reduces SAR. Tests were carried out on flexibility and on-body behavior.
[27] 2009	Higher mode microstrip patch antenna (HMMPA)	Rigid and 3D	2.45	By including shorting vias, the electric fields are engineered to be perpendicular to the surface of the body and thus enabling better on-body propagation. Total height is λ/20.
[28] 2014	Monopole over 2 × 2 AMC	Standard PCB etching on flexible thin layers with foam spacer	2.4	AMC is anisotropic as fields are only in one orientation. The AMC acts as the main radiator and the monopole balances reactance. Design can be bent and reduce SAR significantly.

Things (IoT) and medical implantable devices and our need to communicate with them [20], [21]. They can be fabricated from textiles, be inkjet printed, be etched on small rigid substrates or thin flexible laminates. If conventional etching techniques are used, the behavior is well known in terms of the detuning and reduced efficiency due to the proximity of the body. This section focuses on textile wearable antennas, which present additional challenges due to the fabrication resolution, the shape changing as the textile bends, and the reduced conductivity and thickness of the conducting part. Table 1 summarizes some of the most cited designs [22]–[28]. There are various techniques to design and fabricate textile antennas [29]. The most common ones are embroidery [30]–[32] and screen printing [20] (see Fig. 1). Different fabrication approaches to wearable antennas are shown in Fig. 2. These wearable antennas are usually planar microstrip type with or without a ground plane. The presence of the body has minor impact on antennas that include a ground plane. However, the performance of antennas without ground planes is strongly affected by the distance from the body. In addition, the antenna can move or crumple, thereby shifting the resonant frequency. If there is no ground plane or just a small ground plane, the efficiency increases as the antenna is moved away from the body. The radiation efficiency is much higher when placed on the low-conductivity fat tissue compared to the higher conductivity of the muscle.

FIGURE 1. Specialist digital embroidery machine at Loughborough University for embroidering conductive threads. The designs can be converted into a picture and then fabricated automatically. It is important to be able to control the machine tensions as the threads are designed for their conductivities not their physical properties. The machine can also control the stitch spacing and direction.

As an example case, we refer to a wideband monopole antenna that was previously designed to work well on the body and at several distances from the body. The monopole consisted of a circle with a partial ground plane only underneath the feedline. The monopole antenna was wideband but

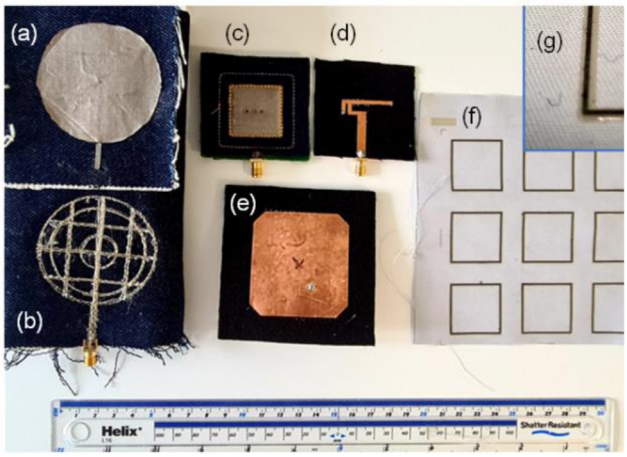

FIGURE 2. Different fabrication approaches to wearable antennas. (a) Nora Dell [125] conductive sheet that can be cut to size, (b) embroidered meshed wideband monopole (note this creates challenges to maintain a 50 Ω transmission line and to ensure a good electrical connection where the embroidered threads cross), (c) combination of Nora Dell, conventional embroidery and embroidered conductive threads, (d) and (e) copper tape on felt, (f) screen printing and inkjet printing on textiles, (g) a zoomed in version of (f); the darker line is the conductive inkjet printed line and either side of that is a screen printed interface line to ensure a flat surface for the thin inkjet layer.

was affected by the body due to the partial ground plane. If the circle of the monopole was increased in size, it would cover lower frequencies. This antenna without the body was very wideband: ~ 2 to > 60 GHz. With the body, the antenna was reasonably well matched from ~ 1.8 to > 6 GHz [6]. Note it was hard to achieve a reflection coefficient, $|S_{11}|$ below -10 dB over a wide frequency band as there are resonant cavities created between the body and the antenna. The antenna was made from a conducting fabric and measured on an adult male person; the results were similar to the simulations but the S_{11} magnitude was slightly worse. This was thought to be due to the sensitivity of the width and hence the impedance of the transmission line. The efficiency increased with larger body-antenna separation and also at higher frequencies (as the separation in wavelengths was increased). For example, at 1.8 GHz, the efficiency was above 60% if the antenna was 20 mm away from the phantom. This highlights the challenges of designing wearable antennas at 1 GHz or even 300 MHz where the antenna is electrically close to the body. A wideband embroidered spiral antenna was previously designed and fabricated, which covered the torso of the person [33]; as the frequency increased, the body became electrically larger and hence the directivity tended to increase.

A related factor to consider is the SAR which is the RF power absorbed per unit mass. SAR limits [34] may put constraints on the amount of power that can be transmitted, which in turn will affect the communication range. Clearly, there is a relationship between the power absorbed by the body and the power radiated. Generally, a ground plane that is greater than one wavelength in size will decrease the SAR but tends to limit the bandwidth [35].

2) Implantable Antennas: Implantable antennas enable wireless medical devices to operate within the body for long periods and are central to wireless technology advancements that bring healthcare home and make it personalized and continuously available [36]–[38]. However, the human body as an operating environment entails key challenges to antenna design. First, all medical implants must be minimally intrusive. This requirement restricts the viable size and structure of the implantable antennas, making their design and fabrication challenging [39]. Second, the biological matter exhibits high permittivity and appreciable conductivity adding to the formidable challenge of achieving acceptable radiation efficiency. Third, the human body presents significant variability between individuals, and it is a complex structure for numerical electromagnetic (EM) simulations.

The biological matter features decreasing and increasing trends in the relative permittivity and conductivity versus frequency, respectively [40]. As a result, due to high path loss, the communication link between an implantable antenna and an external receiver becomes unfeasible beyond the low-GHz frequencies [41], [42]. The main reason is the rapidly increasing propagation loss versus the frequency experienced by the EM wave traveling inside the body [41], [43]. Specifically, this means that although the electrical size of an implantable antenna can be increased by increasing its operating frequency to, e.g., cm-wave frequencies, this is not a viable approach to improve the system's overall performance [5]. On the other hand, implantable antennas will be electrically small in the low-GHz range and subject to the corresponding performance bounds.

In addition to the applicable frequency range, the dielectric properties of the human body are decisive to the radiation properties of implant antennas [43]–[45] (see also Section II-D). First, the radiation efficiency and off-body radiation pattern are functions of the propagation loss associated with the EM wave propagation inside the body and the reflection of the wave that impinges the body surface. In other words, they depend on the implant's depth and orientation which are fixed by the application. In particular, the upper bound of the radiation efficiency will depend on the depth of the implant. Thus, the most effective way an antenna designer can contribute to the overall performance of an implantable antenna is by minimizing the near-field loss and the impedance mismatch loss [45]. Since the biological matter is non-magnetic, antennas that store a more significant portion of the near-field energy in the magnetic field than electric field are more favorable [43]–[45].

Article [44] exemplifies the computation of the contribution of the near-field loss, propagation loss, and reflection loss on the radiation efficiency of an implantable antenna enclosed in a spherical body phantom, as shown in Fig. 3(a). Assuming the simulation settings summarized in the figure caption, the authors obtain the radiation efficiency shown in Fig. 3(b). Towards lower frequencies, roughly below 500 MHz, the near-field loss significantly decreases the radiation efficiency. As the frequency increases, propagation loss

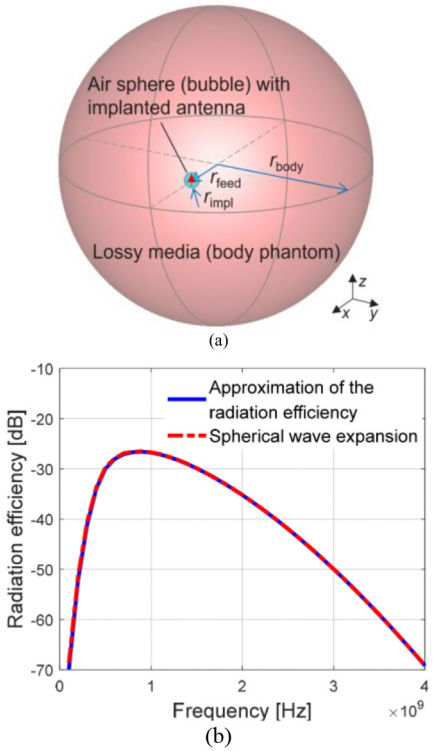

FIGURE 3. Radiation efficiency of a Hertzian dipole with $r_{feed} = 0$, $r_{impl} = 5$ mm, and $r_{body} = 10$ cm in a spherical muscle phantom from article [44].

becomes the predominant loss source. Because the implant is at a deep location, the propagation loss dominates over the reflection loss. However, for a shallower implant, the reflection loss would become relatively more important.

Whereas creating efficient sub-cm-sized implantable antennas is challenging, developing wireless medical microelectronic systems in the same size range is comparatively more straightforward. Thus, an implanted microsystem may contain advanced wireless communications modules. This trend has prompted the growing demand for electromagnetically advanced implantable antennas that support, e.g., the multi- or broad-band operation. For this purpose, multiple frequency bands, including the Medical Implant Communication Service (MICS) band between 401 MHz and 406 MHz, the MedRadio comprising the multiple subbands between 401 MHz and 457 MHz, and the Industrial, Scientific, and Medical (ISM) bands centered at 915 MHz and 2.45 GHz, are available, depending on the geographical location. For example, in [46] authors report a conformal capsule slot antenna with a wide impedance bandwidth ranging from 1.64 to 5.95 GHz (113.6%). Authors in [42] compare the performance of implantable antennas operating in these bands, highlighting how antenna miniaturization may come at a compromise of reduced electromagnetic performance. In addition, circularly polarized antennas (CP) downsized to a clinically viable size for implantation, and the RFID-inspired implant communications have been considered. The remainder of this section reviews the recent trends in implantable antennas through several designs summarized in Table 2.

The recent works [47]–[51] on dual-band implant antennas demonstrate several practical design approaches for implantable antennas. The presented antennas are planar inverted-F and microstrip patch antennas, which permit various miniaturization approaches. Central to all designs [47]–[51] is the location of the shorting pin and slots patterned to the radiator and ground plane. Together, they modify the current path suitably to establish the two desired resonance frequencies. In addition, all designs [47]–[51] include a superstrate layer. It serves as a low-loss buffer material between the radiator and the biological environment. Moreover, antennas in [47], [49], [51] use a high-permittivity material in the superstrate and substrate to help lower the resonance frequency of the antenna.

In addition to the innovative design of the antenna's internal structure that maximizes the implant's EM performance (e.g., dual-band operation), the external shape of the antenna is crucial to the application. A round exterior shape that avoids sharp corners helps to minimize the intrusiveness of the implant [47], [49]. A bio-compatible superstrate layer can form the encapsulation of the device [48] to simplify manufacturing and reduce the device thickness. In terms of the effective use of space, the associated electronic circuitry can be integrated with the antennas, as demonstrated in [49], where the antenna and rectifier share the same ground plane. For the proper system integration of wireless implantable devices, optimizing the antenna considering all other modules present within the same package, as in [50], provides the most holistic design approach.

Based on the design approaches discussed above, the authors of [52] and [53] have created triple-band implantable antennas based on spiral-shaped radiators. Both designs make use of a high-permittivity substrate and superstrate and slotted ground plane. In contrast to the Planar Inverted-F Antenna (PIFA) [53], the antenna [52] does not include a shorting pin and thus is not a PIFA. The sizes of the antennas [52] and [53] are $7\times6.5\times0.377$ mm^3 and $\pi\times(11.2\text{ mm})^2\times0.5$ mm, respectively. The corresponding measured peak gain values are -30.5 | -22.6 | -18.2 dBi and -23 | -20.5 | -19 dBi at the frequencies of 402 MHz, 1600 MHz [1] / 1430 MHz [2], and 2.45 GHz. The considered implant location was 3 mm and 4 mm in the scalp, respectively. Relative to the size, both antennas reach the state-of-the-art gain performance together with the triple-band operation.

In the works [54] and [55], the authors have focused on improving the impedance bandwidth of dual-band PIFA. This was realized by using spiraled radiators divided into two branches relative to the feed point. In [54], one of the spiral branches was shorted to the ground, making the radiator of the same type used in [53]. In [55], one branch of the spiral was shorted at its endpoint. In [54], several narrow slots were cut in the ground plane, but in [55], a single large rectangular slot was employed. The two works demonstrated

TABLE 2. The main features of the implantable antennas discussed in Section II-A1.

Ref. Year	Antenna structure	Freq. (MHz)	Volume (mm^3)	Depth Tissue	Gain (dBi)	CP
[47] 2019	Circular PIFA(*)	402 2450	$\pi \times (5.35)^2 \times 1.34$	3 mm Skin	–41.0 –21.3	No
[48] 2018	Patch w/ a flower-shaped radiator(*)	928 2450	$7 \times 7.2 \times 0.2$	50 mm Skin	–28.4 –25.7	No
[49] 2019	PIFA	402 915	$16 \times 14 \times 1.27$	10 mm Muscle	–35.9 –24.3	No
[50] 2019	Slotted patch /w a shorting pin(*)	915 2450	$7 \times 7 \times 0.2$	3 mm Head	–27.7 –23.0	No
[51] 2020	Circular patch w/ a shorting pin(*)	403 915	$\pi \times (5.35)^2 \times 1.28$	10–16 mm Muscle	–31.6 –33.1	No
[52] 2019	Spiral-shaped patch(*)	402 1600 2450	$7 \times 6.5 \times 0.377$	3 mm Scalp	–30.5 –22.5 –18.2	No
[53] 2021	Spiral-shaped circular PIFA(*)	402 1430 2450	$\pi \times (11.2)^2 \times 0.5$	4 mm Skin	–33.3 –21.9 –19.6	No
[54] 2019	Spiral-shaped PIFA(*,#)	402 2450	$9 \times 11 \times 0.5$	3 mm Skin	–34.6 –18.7	No
[55] 2018	Spiral- shaped PIFA(*,#)	403 2450	$14 \times 17 \times 0.25$	Thorax	–33 –16	No
[56] 2019	Split-ring loaded loop(#)	403 433 915 2450	$18 \times 18 \times 1.24$	GI tract	–34.3 –30.6 –26 –18.4	No
[57] 2014	Circular slotted patch w/ capacitive loading	2450	$10 \times 10 \times 1.27$	4 mm Skin	–22	Yes
[58] 2018	Patch w/ capacitively coupled stubs	915	$11 \times 11 \times 1.27$	4 mm Skin	–29	Yes
[59] 2018	Slotted patch /w a shorting pin(#)	915	$\pi \times (4.7)^2 \times 1.27$	4 mm Skin	–32.8	Yes
[60] 2019	Meandered loop on periodic surf.	920 2450	$10 \times 10 \times 0.6$	2 mm Skin	–29.3 –21	Yes
[61] 2018	PIFA loaded w/ metamaterial	915 2450	$7 \times 6 \times 0.254$	4 mm Skin	–17.1 –9.8	Yes
[62] 2020	Slotted patch(*,#)	915 2450	$6.5 \times 6.5 \times 0.05$	50 mm Muscle	–28.2 –24.5	Yes
[63] 2019	Slotted patch w/ 2 shorting pins(#)	2400	$9.8 \times 9.8 \times 1.27$	3 mm Skin	–33	Yes
[64] 2021	Circular slotted patch w/ a shorting pin(*,#)	2400	$\pi \times (4)^2 \times 1.27$	4 mm Skin	–37.4	Yes
[65] 2020	Circular slotted patch /w 2 shorting pins(#)	2450	$\pi \times (4.8)^2 \times 1.27$	3 mm Muscle	–20.3	Yes
[68] 2020	Ellipse-shaped double split-ring	915	$\pi \times (3 \times 1.5) \times 1$	16 mm CSF	–25.7	No

(*) Slotted ground plane. (#) Broad- or wide-band operation.

the significant fractional bandwidths of 38% [54] and 40.8% [55] at the frequencies of 402 MHz and 2.45 GHz, respectively.

The authors of [56] took a different approach to bandwidth enhancement. Instead of a grounded antenna, they developed an 18×18 mm^2 planar loop antenna coupled with two double

split-ring resonators (SRR). The structure was folded onto the surface of a cylinder-shaped implantable capsule (radius of 3.2 mm) that contains other electronics modules. The SRRs not only had a positive influence on the impedance matching, but they also suppressed the near electric field of the antenna. This enhanced the radiation efficiency and reduced the specific absorption rate. In terms of the EM performance, the antenna achieved the substantial impedance bandwidth ($|S_{11}| < -10$ dB) from 307 MHz to 3.5 GHz, and its realized gain increased steadily from -34.3 dBi at 402 MHz to -18.4 dBi at 2.45 GHz.

The first CP implantable antenna, operating at 2.45 GHz ISM band, was presented by Liu *et al.* in 2014 [57]. The antenna ($10\times10\times1.27$ mm^3) was developed from a microstrip patch antenna with a square slot cut at the center of the radiating patch and truncating two corners of the slot. This produced the CP property while additional slots in the radiating element provided reactive loading and increased the current path to achieve the compact size. Until now, the research on implantable CP antennas has produced numerous advancements, such as attaining the CP operation at 902 MHz [58], [59] dual-band 902/2450 MHz CP antennas [60]–[62], as well improvements to the axial ratio bandwidth [59], [63]–[65]. As a new design feature, metasurfaces were utilized in [60], [61].

To return to integrating antennas with the medical implants, sometimes the required electronics can be implemented as microsystems instead of cm-sized modules. In this regard, the passive ultra-high frequency (UHF) RFID technology [11], [66] is considered a compelling approach to battery-free implants. Due to the power-efficient mechanism of the modulated scattering used in the uplink (tag-to-reader) communications, RFID enables ultra-low-power microsystems that operate on the energy they harvest from the reader's RF signal. The articles [4], [67], [68] present two different antenna concepts for RFID-inspired brain implants. In the first approach [4], [67], the implant within the cranial cavity comprises a circular loop connected with the RFID microsystem. The loop couples through the EM near-field to a larger wearable split ring resonator. Together the two parts form a spatially distributed antenna system with the gain of -18 dBi at 915 MHz (implant depth: 10 mm). In the second approach [68], the system comprises only an elliptic cylinder-shaped implant ($\pi \times (3 \times 1.5) \times 1$ mm^3) based on a double split ring antenna where the RFID microsystem connects to one of the rings, and a capacitor loads the other one. The gain of the antenna at 915 MHz was -25.7 dBi (implant depth: 16 mm). In both approaches, the housing of the implant was formed by a low-permittivity bio-compatible material.

2) INDUCTIVE TELEMETRY

The data communication link in implantable medical devices (IMD) encompasses a downlink from a base station (BS) to an IMD and uplink in the reverse direction [69]. Traditionally, data communication for IMDs is achieved using an inductive coupling link at low frequencies, typically below 50 MHz. At those frequencies, inductive links have been used for short range implants applications such as pacemakers, intra-ocular, and muscle stimulators [70], [71]. The principle of operation for inductive coupling is based on the mutual inductance through the magnetic flux between an implantable coil, or antenna, and wearable or close to the body coil, or antenna (Fig. 4) [72], [73].

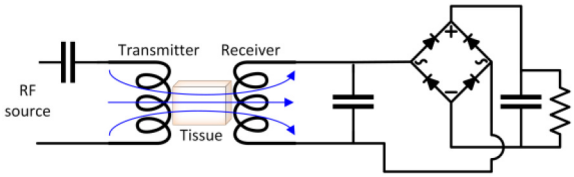

FIGURE 4. A generalized inductive telemetry link with coils, where receiver is the implantable side, typically operates below 50 MHz.

When an implantable antenna is interrogated by an exterior antenna, dielectric properties of tissues result in power absorption, particularly for the electric field [74], [75]. In contrast, the magnetic response is usually weak since the magnetic permeability of most tissues is equivalent to free space ($\mu = \mu_o$) [76]. For this reason, inductive coupling is a favorable method for power transfer to battery-less IMDs (Fig. 4). The coupling is predominately achieved through magnetic field leading to reduced interaction between the EM field and the surrounding biological tissues. The reading distance between exterior and implantable antennas falls in the near-field region [77], [78]. Generally, the inductive coupling link between exterior and implantable antennas is modelled as a lossy two-port network. The implantable side is tuned in parallel or series to the load by a capacitor, whilst the external side is normally tuned in series with a capacitor. Increasing the coupling coefficient leads to a reduction in the injected current at the external coil and reduction in losses. Therefore, a high coupling coefficient is required by increasing the mutual inductance of external and implantable coils [79].

Unlike far-field EM simulation, where the wireless link can be investigated separately from antennas, the link between exterior and implantable antennas needs to be incorporated in the modeling and design of inductive links [80]. The generally used metric to quantify the performance of the wireless power link is the power transfer gain, which is the ratio of the power delivered to the load and the power supplied to the exterior coil, i.e., accepted power. When the input impedance and output impedance are conjugately matched to the source and load respectively, the maximum operating power gain is achieved [81]. The difference between operating and maximum operating power gain is that the latter neglects the mismatch between the implantable coil and an integrated load [82]. However, in practice, fabrication inaccuracies alter the conjugate matching and impedance mismatch loss occurs.

Merging data communication and WPT in the same frequency can lead to interference. In turn, either maximizing WPT or data communication as simultaneous optimization is cumbersome. The requirements for WPT and inductive telemetry are paradoxical [83]. High power efficiency can be achieved with resonant coils at low frequencies, which hinders achieving high data rate by limiting the available bandwidth [84]. Therefore, different techniques have been used to support high data rate and high WPT by using different coils, mainly arranged in an orthogonal way to support high data rate and efficient power transfer [85], [86]. In this case, the requirements for data rate and WPT can be addressed separately [86]. Alternatively, using same coils for data rate and WPT can be achieved by optimizing the design requirements which can be a challenging procedure. In [87], the authors propose using two pairs of coils for inductive wireless link and pair of antennas for back telemetry. In this regard, the requirements of data rate and power efficiency are not compromised at the expense of increasing the overall footprint of the IMD.

The modulation techniques for data communication often employ constant amplitude modulations (i.e., frequency or phase modulations) to provide uninterrupted power flow for IMDs [88]. However, an onboard clock and carrier synchronization are necessary for accurate data retrieval, which increases the power consumption for IMDs. On the other hand, amplitude modulation has the advantage of simplicity with less power requirements as clock and data retrieval are achieved by data sequencing [89].

Recently, there has been significant research into the potential of increasing the operating frequency of inductive link to above 100 MHz. Those investigations aimed at utilizing the advantage of high frequencies for high data rate, small antenna size (mm-size) and improved power transfer efficiency by operating in the radiating near-field rather the reactive near-field [90]. At such high frequencies, antennas are designed instead of coils for inductive telemetry to operate efficiently at high frequencies.

When designing a mm-size implantable antenna, the input high reactive impedance is matched to a high capacitive input impedance of an integrated chip/load to maximize the power transfer efficiency [91]. However, it is challenging to achieve a perfect conjugate matching between the antenna and chip/load, hence, the mismatch loss needs to be considered when calculating the power transfer efficiency. In [92], an inductive coupling link was proposed for an 8 mm^3 3D cube implantable antenna coupled to an exterior copper fabric and embroidered loop antennas. The link was designed at 300 MHz and measured in a head-equivalent liquid phantom. *In vitro* tests of the inductive coupling link for a 1 mm^2 planar antenna were reported in [80] with a simple multilayer tissue model used in the simulation.

In [93], a 1 mm^3 3D cube antenna was designed at 400 MHz, however, the measurement of the wireless link was performed in air only, which does not reflect the actual link losses exhibited by the high relative permittivity of head tissues that was considered in [94]. A multi-turn 3D implantable coil was optimized in [95] using a single tissue model for the operation at 100 MHz at the expense of increasing the exterior antenna dimension. Using a mm-size implantable antenna necessitates the use of matching circuits to properly feed the antenna, hence, the design of matching circuits should be optimized in order not to adversely affect the bandwidth.

It is worth mentioning that inductive telemetry is therefore not standardized, and the choice of the operating frequency is dictated by the design requirements and application instead of well-defined guidelines [71]. Table 3 shows a summary of recently reported inductive coupling links operating at sub-1 GHz band (100 MHz-1 GHz) [9], [93], [94], [96]–[101].

TABLE 3. Summary of some reported inductive coupling for sub-1 GHz links (100 MHz-1 GHz).

Ref. Year	Operating frequency	Efficiency @ mm	Implant design	Verified in
[96] 2016	200 MHz	0.56% @ 12 mm	mm-Size solenoid	Beef
[97] 2019	237 MHz	0.026% @ 12 mm	Spiral coil	Bovine muscle
[94] 2018	400 MHz	0.08% @ 15 mm	mm-Size bowtie antenna	Piglet
[93] 2017	400 MHz	0.1% @ 10 mm	mm-Size cube antenna	Air
[98] 2015	403 MHz	5.24% @ 10 mm	Split ring resonator	Minced pork
[99] 2018	430 MHz	0.16% @ 60 mm	Spiral coil	Skin phantom
[100] 2018	432.5 MHz	13.9% @ 10 mm	Spiral coil	N/A
[101] 2015	915 MHz	0.04% @ 16 mm	mm-Size cube antenna	Head phantom
[9] 2018	915 MHz	1.93% @ 50 mm	Spiral coil	Minced pork

B. WIRELESS POWER TRANSFER

The mode of operation for IMDs can be broadly classified based on the power source into three categories: active, passive, and semi-active [102]. IMDs which have embedded batteries fall in the first category, while passive IMDs operate from an exterior power source via WPT [103]. The semi-passive, or often named semi-active, IMDs use a hybrid combination of an on-board battery and exterior interrogator, which modulates the antenna input impedance via a switch [104].

As an IMD is located inside biological tissues, EM radiation is absorbed and converted into heat [105]. Therefore, safety precautions limit the input power to IMDs, which in turn affect the communication range. Moreover, EM radiation is governed by the dielectric properties of tissues. Hence, accurate dielectric characterization and modelling of biological tissues have a great significance in understanding and simulating EM radiation of IMDs in the human body [106], [107] (please refer to Section II-D).

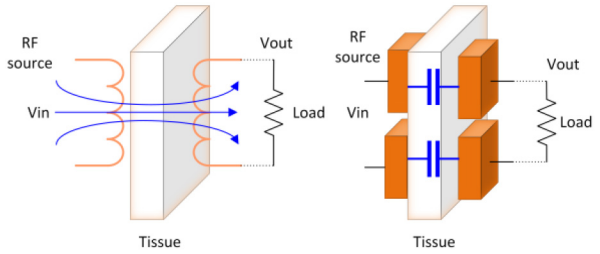

FIGURE 5. Inductive versus capacitive coupling through biological tissue. The coupling in inductive link is achieved via magnetic field, whereas in capacitive link is achieved via electric field.

To permit long-term implantation and reduce subsequent surgeries for drained battery replacement in IMDs, WPT through a power link is becoming increasingly popular [103]. There are different modalities for WPT in battery-less IMDs, namely near-field resonant inductive, capacitive, galvanic, mid-field, far-field WPT links. Besides that, there are other modalities utilizing ultrasound, optical waves, and molecular communication [70].

To achieve higher efficiency for resonant inductive WPT, the quality factor of used coils or antennas should be high to condense the power in the near-field, which limits the data rate. It is necessary to operate inductive coupling at lower frequencies (Fig. 5), especially when the link is designed for efficient power transfer to IMDs [108]. The losses of the propagation channel due to biological tissues are in consonance with frequency [109]. On the other hand, higher frequencies aid the miniaturization of the antenna as compared to the high frequency (HF) range used extensively in inductive coupling for IMDs. Recently, there has been a considerable attempt to extend the inductive coupling operating frequency to UHF [88]. Miniaturization of the antenna by means of a higher frequency is obtained, yet impedance matching is achieved using lumped components [8]. As evident from the analytical and numerical simulations in [90], for mm-size implantable antennas, sub-GHz and low GHz range provide the optimal frequency to maximize the link gain depending on the dimension of the exterior antenna. In this case, the inductive coupling operates in the mid-field WPT, which is regarded as a holistic combination of a typical inductive near-field and radiative far-field for mm-size implantable antennas [103]. Higher frequency bands are utilized to overcome the drawbacks of low frequency wireless links between an exterior reader and IMDs. Therefore, near-field WPT links are envisaged for mm-size implantable antennas to further reduce the overall volume of the implantable antenna to 1 mm^3 [110], [111]. In fact, the operating frequency should represent a good compromise to obtain a compact exterior antenna, acceptable penetration in tissues and satisfactory power transfer to a miniature battery-less medical device with an acceptable inductive coupling to the exterior reader [95].

In another way to realize WPT to IMDs, capacitive coupling has been investigated, with a caution on safety aspects (Fig. 5) [112]. Capacitive coupling is created by displacement and conduction currents when exterior capacitive patches are driven by a time-varying voltage source and placed near implantable capacitive patches [113]. In biological tissues, the capacitive reactance between exterior and implantable patches is high, which limits currents and WPT. Hence, it is not a preferable WPT modality for IMDs, as it needs a higher rate of electric field change or a wide surface area for coupling patches [114]. In fact, capacitive coupling is equivalent to a parallel capacitor with a sandwiched tissue as a dielectric. The dielectric loss resistance varies proportionally with the separation distance (i.e., tissue thickness) between exterior and implantable capacitors. Furthermore, IMDs can suffer from a large size due to the size of capacitor patches. Hence, it is primarily used for near-surface transcutaneous implant communication and not for deep implants [114].

This principle is different from inductive coupling, which takes the advantage of non-magnetic response of tissues. For mid-field WPT, the frequency is optimized to achieve higher coupling for miniature implantable antennas (i.e., in mm-range) [110]. The separation between exterior and implantable antennas is around one wavelength. The frequency of weakly-coupled antennas is obtained in low-GHz and GHz range depending on the size of the exterior antenna [90].

Galvanic coupling based on volume conduction theory (propagation of the electric field in lossy conducting tissues by induction current) is particularly used for intra-body communication and not IMDs [115]. Galvanic coupling still poses a high path loss (in order of more than 40 dB) in muscle tissue at 13.56 MHz, while the receiver is placed at a distance of around 5 mm in air [115]. Placing an exterior receiver for an IMD in air is prone to fade the conduction current, which in turn increases the path loss.

In far-field WPT, the exterior and implantable antennas are far apart from each other by at least two wavelengths. Hence, the radiated EM fields will be plane waves [78]. On the contrary, the near-field propagation in biological tissues is complex as EM field also consists of non-radiating waves, i.e., standing waves. This can facilitate the study of far-field WPT as antenna gain is defined for the far-field case and the path loss follows Friis' equation, which can simplify the study of far-field WPT compared to near-field [116]. Nevertheless, far-field WPT suffers from low power efficiency and can be made feasible with the support of focusing lenses, exterior antenna arrays or parasitic wearable conductors [117]. In particular, far-field WPT for IMDs requires another dimension of complexity to the system in order to provide adequate power to IMDs without violating the safety standards, which is deemed impractical for IMDs. Overall, WPT based on inductive coupling is the most used WPT modality for IMDs due to its advantages in terms of penetration in biological tissues, despite its short operating distance and sensitivity to misalignment between external and implantable counterparts.

C. MATERIALS AND FABRICATION

1) EMERGING MATERIALS

1) Emerging Materials for Wearables:

Fabric Substrates and Conducting Elements: The properties of dielectrics and fabrication methodologies for conducting textiles have been reviewed in [118]. Textiles tend to have low relative permittivity ($\varepsilon_r \sim 2 - 3$) and have low losses. Therefore, they do not assist in miniaturizing the antenna and they do not have an adverse effect on the efficiency. Another problem arises if the fabric antenna is expected to operate in rainy or wet conditions as this will absorb water and affect antenna efficiency by changing the substrate's effective permittivity and loss tangent [119], [120].

Embroidered antennas generally use fabric and conductive threads to form the antenna structure [121], [122]. These can be aesthetically or covertly integrated into clothing and manufactured as individual unique elements or mass manufactured. This leads to an embroidered antenna design that is quite flexible and unobtrusive to the wearer. Embroidery lends itself to antennas where the metallization is linear rather than covering a large continuous area. These conducting threads are difficult to embroider and a specialist embroidery machine is required to control the different tensions [123], [124]. The stitch spacing and direction is important, as this changes the sheet resistance and thus influences antenna efficiency [121], [122].

However, the antenna efficiency is compromised as the metallization has a limited conductivity and thickness [122]. For example, some of the most popular threads consist of a polymer core with a 1-micron thick metalized exterior. To enable the metal layer to adhere to the polymer core, a mixture of metals is used. It is noteworthy that each thread contains multiple filaments. By comparing the measured results to simulations, the conductivity has been ascertained to be approximately 1 MS/m. The skin depth effect of the embroidered thread that reduces the antenna efficiency becomes more significant at lower frequencies and hence the antenna efficiency decreases at lower frequencies (even before the body is considered). The electromagnetic behavior can be improved by increasing the number of embroidered layers or the stitch density, however, this comes at the cost of increased weight, reduced physical flexibility / comfort, and increased cost of raw materials.

Similar issues exist with other conducting textiles as their fabrication is inherently optimized for flexibility and manufacturability rather than the RF performance. Conductive fabric sheets are available; one example is "Nora Dell" from Hitek Ltd. [125] which is a three-layer fabric composite with a quoted sheet resistance of 0.009 Ω/m^2. In other cases, antennas on textiles have been created by screen printing an interface layer onto cotton and then inkjet printing the conducting layer [126], [127]. The dielectric interface layer provided a flat surface for the conducting ink and hence was required to achieve conducting lines. The metallization was approximately 1 μm thick with a conductivity of $\sim$ 1 MS/m and hence was very similar to an embroidered thread. This was an effective way of making a lightweight conducting textile with bespoke designs. However, further work would be required to test the robustness to bending and stretching.

Anisotropic Substrates and Superstrates: The term anisotropy describes materials which have different relative permittivity, relative permeability, loss tangents, or conductivity values in two or three different axes. Recently, there has been increased research interest in the physics and design of anisotropic or extremely anisotropic structures. However, studies on modelling, characterization, and practical applications of anisotropic artificial dielectrics at microwave frequencies are limited. Until recently, commercial EM software was unable to consider anisotropy of homogeneous materials. It is increasingly important to measure anisotropy at higher frequencies where the internal feature size of conventional materials becomes more significant [128]. Several articles discuss the potential advantages and applications of exploiting anisotropy including control of the frequency and bandwidth, modifying the radiation patterns, lenses, beamforming, microwave resonators, reducing surface waves, and minimizing the antenna profile [128]–[130]. Textiles are naturally anisotropic, and the relative permittivity is different parallel to and perpendicular to the thread direction. However, the difference for most materials is less than 10% and hence the effects of the anisotropy are not very significant [131].

Tuovinen *et al.* have considered anisotropic substrates via simulation [132]. In [132], vertical strips rotated by 45 degrees were used to create anisotropic substrates for ultra-wideband (UWB) on-body antennas. The anisotropic substrates increased the gain at boresight and removed the nulls and smoothed the radiation patterns. Structures were simulated as homogeneous anisotropic substrates and also as thin strips. This anisotropy could be achieved via 3D printing the layers and could be used to minimize the pattern nulls of a wearable antenna on the human body.

Metamaterials: Metamaterials and metasurfaces can be designed to prevent the propagation of waves. They are also used in some wearable applications to reduce the back radiation and, hence reduce the absorption in the body and improve the antenna efficiency [133]–[135]. Artificial magnetic conductors (AMCs) control the phase of the reflection from the surface, hence reducing the destructive interference of the reflected. This enables the profile of the antenna to be reduced while maintaining a high efficiency [136]. The example in [135] showed a gain improvement of 1.9 dB and a backward radiation reduction by 8 dB with the introduction of an AMC. The disadvantages of this are that (i) the system requires an extra layer of conductor and dielectric, (ii) the bandwidth is limited, and (iii) the ground plane typically needs to be two wavelengths across which makes the overall antenna size quite large, especially at 1 GHz or below. In [137], authors describe an electrically small antenna employing an AMC substrate, both fabricated by using an inkjet-printed solution, for sub-GHz applications.

In another case [138], the use of metamaterials is explored to improve the penetration of the electric field inside the human body for diagnostic/therapy applications. The work addresses the problem of designing a thin matching layer based on a metasurface to increase the electric field penetration into muscle tissue for various scenarios. A wider literature review on AMCs for wearable antennas can be found in [139].

Textile antennas which incorporate metamaterials have been considered [22], [140]. In addition to the challenges of rigid metamaterials, these flexible versions also suffer in practice as bending or compressing the layers further reduces the bandwidth. An example is shown in [141] which uses an AMC with a wideband "windmill-like" antenna which provides a wide return loss bandwidth of 5.7 – 11 GHz (fractional bandwidth, FBW: 63.4%) with a peak gain of 8 dBi (at 7 GHz). The efficiency values of 90.6 %, 83.8 % and 85.5 % are achieved at 7 GHz, 8.5 GHz and 10 GHz respectively. The size of this AMC is 0.874 λ_{max} × 0.874 λ_{max}; when scaled to 1 GHz the AMC would be 26.2 cm × 26.2 cm.

A different metamaterial antenna concept for wearables has been discussed in [28]. The concept is to use the AMC in the frequency range where the reflection phase is + 90° so that it behaves like an inductive surface. A monopole is then placed near the AMC layer and designed to operate below its fundamental mode and hence the monopole impedance is capacitive. Therefore, the reactances cancel out and a good impedance match can be achieved for the overall system. The key point is to locate the main electric fields on the edges of the monopole and in the slots of the AMC. These gaps behave like slot antennas (magnetic sources) and these can be located close to the ground plane due to image theory. Here the AMC itself becomes the main radiator. Several slots can be used to create an array with a tapered amplitude with the central slot providing the strongest radiation. This concept is advantageous over conventional AMCs as the footprint can be reduced to only require a 2 × 2 array which can be much smaller than 2 λ as typically required for AMCs. The antenna had a high front to back ratio; hence exhibited robustness to placing objects nearby, low SAR and high efficiency. This antenna in [28] was designed for 2.4 GHz and achieved a 6% fractional bandwidth. The size including the AMC was 0.5 λ_{max} × 0.3 λ_{max} × 0.028 λ_{max} [28]. It used an anisotropic AMC to save space as the monopole was linearly polarized and the AMC was only required to operate in one axis.

2) Emerging Materials for Implants: Implantable medical electronics require materials with appropriate electrical, mechanical, and biological properties. High electrical conductivity materials are used for transducing electrical signals between the biological tissues and electronics, such as wires, antennas, ground planes, etc. Typically conductivities at least on the order of 10^4 – 10^5 S/m are needed for medical electronics [142], although antennas with conductivities as low as 5 x 10^2 S/m have been proposed [143]. Insulating materials separate these conductive materials from body tissues, isolate individual electrical components, and protect the conductive materials from biological corrosion [144], [145]. This section describes existing and emerging materials for bioelectronic applications.

Both conductive and insulating implantable materials need to be biocompatible for chronic or acute applications. The definition of biocompatibility is highly dependent on the application. For chronically implantable (long term) electronics, materials must be chemically inert under physiological conditions throughout the lifetime of the implant. Recent developments in transient implantable electronics have raised interest in materials that can be biodegraded under physiological conditions without creating toxic byproducts [146]–[149]. Insulating materials are typically polymeric or ceramic materials, both of which have been FDA approved [150]. For conductive materials, noble metals [151], [152], such as titanium and gold, are often used for chronic applications. Non-toxic and biodegradable metals such as magnesium, silicon, iron, carbon nanotubes [153], [154], and graphene [154] have also been used. Other creative approaches may use natural body fluids as part of the material. Compatibility with MRI scans also needs to be considered, requiring the use of non-magnetic particles.

In addition to biochemical compatibility, mechanical compatibility between the tissue and the implant can be improved by making them soft and compliant rather than stiff and hard. Conventional metallic materials have a high mechanical mismatch with biological tissues. Alternative soft conductive materials proposed for medical electronics include biocompatible versions of paints [155], [156], conductive adhesives [157], polymers [151], [158], [159], hydrogels [151], inks [160] and fluidic conductors [161]. The effective conductivity of the material is controlled by the conductivity of the material (fluid, ink, etc.), as well as how it interacts with the body. Some tattoo inks, for instance, are highly conductive [162], but the tattoo itself may not be, as the different cellular components uptake the ink nanoparticles, placing insulating cell walls between the conductive particles [163]. Materials also need to be thick enough to accommodate the electrical skin effect, which can be a problem for inks and paints. Some of these materials can potentially be injected as fluids and converted to soft solids with heat (either from natural body heat or heat provided by a coaxial applicator). This could open up the possibility of producing new types of antenna structures directly in the body [12], [151].

2) ADDITIVE MANUFACTURING

Despite revolutionary developments in the fields of wearables and IoT technologies (Fig. 6), the design of wireless wearable systems remains challenging, and largely dependent on several factors such as device size, manufacturing methods, material compatibility and, most importantly, the available source of power. Additive manufacturing techniques (AMTs), such as inkjet and 3D printing, offer a surprising wealth of

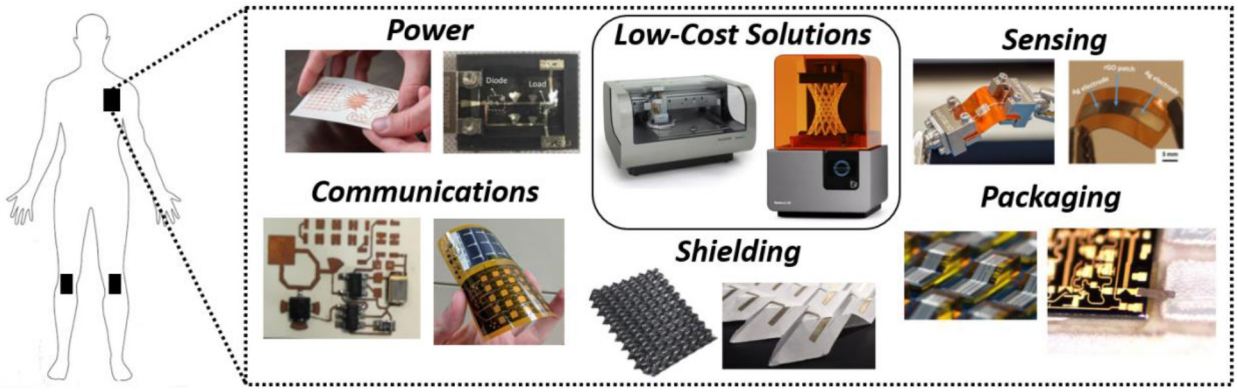

FIGURE 6. The enabling role of low-cost additive manufacturing techniques in the development of wireless wearable systems.

solutions for the aforementioned needs of wearable devices. While traditional lithographic manufacturing techniques are the main contributor to the growing wireless electronics industry, they suffer from multiple drawbacks such as long turnaround times, extensive design verification requirements, and the production of harmful waste. A new industrial revolution is seeking environmentally-friendly solutions, fast prototyping and 3D complex structures. 3D printing is considered a key enabler of this movement, with its ability to unlock the use of two additional dimensions, and the introduction of features that are otherwise unreachable using traditional manufacturing methods. 3D printing is known as an additive technique since the designs are typically built up, rather than etched or milled, leading to a large reduction in waste material and tooling: only the material that is necessary is printed. With the continuous improvements in 3D printing technologies such as micro stereolithography, high precision and resolutions down to several microns can now be realized, making it compatible for applications requiring mm-wave and beyond. Another important feature required for the realization of printed wireless electronics at RF and mm-wave frequencies is multi-material (conductors, semi-conductors, and dielectrics) capability. Inkjet printing, a subset of additive manufacturing, operates based on a Drop on Demand concept, where the ink is disposed onto the substrate using an ink cartridge consisting of an array of nozzles with individual piezoelectric elements. Combined in one system, inkjet and 3D printing enable the development of smart heterogeneous architectures involving antennas, RF/mm-wave circuits, interconnects, sensors, microfluidic channels and more [9], [10].

AMTs are not limited to specific materials or substrates and have been demonstrated to be successful and often superior on multiple scales ranging from systems, to packages to dies and finally individual components. On the system scale, cutting-edge mm-wave structures were realized on flexible Kapton polyimide, Liquid Crystal Polymer (LCP), and Teflon/PTFE substrates, with printed silver nanoparticles (SNP), gold, graphene, and polymer-based inks, demonstrating ultra-low power communications at km ranges and the potential powering of IoT and wearable sensors at >100 m away from a 5G base station [164]–[166]. With the need for power sources remaining the centerpiece in the hardware design of wearable devices, and the use of batteries critically restricting the extent and scope of the application of such valuable devices, wireless power transfer offers an environmentally-friendly, efficient, and non-interrupted operation. Moreover, origami-infused EM structures - impossible to realize with conventional manufacturing processes - were fabricated on paper substrate achieving a combination of low cost, reconfigurability, flexibility and ease of fabrication [167]. These shape-shifting electromagnetic structures offer shielding, filtering and reconfigurability, required for wearable systems in an on-body setting. On the package and die levels, hybrid manufacturing - inkjet and 3D - has enabled the implementation of smart multi-function System on Package (SoP), System in Package (SiP) modules with intelligent interconnects and encapsulation, demonstrating a performance superiority over traditional packaging methods such as ribbon bonds and wire bonds [168]. On the component level, the multilayer deposition of materials with different conductive properties allowed the realization of fully-printed passive and active devices in additive to ultra-sensitive chemical, gas, humidity, and temperature sensors based on printed functionalized carbon-nanotubes (CNTs) ink [9].

These breakthrough implementations enabled by additive manufacturing techniques unlock the ability to develop low-cost, zero-power, smart and responsive health and bio-monitoring devices capable of communicating real-time health data at long-ranges while being completely conformal, bendable, and compatible with the human skin.

D. EVALUATION

1) EVALUATION TECHNIQUES AND TISSUE PROPERTIES

Experiments with human-body physical phantoms are indispensable to validate the results of numerical simulation or to avoid animal experiments particularly for implantable antennas. The validation and testing of antennas used in bioelectromagnetics applications are done using materials

that mimic the electrical properties (ε_r and σ) of the human tissues [14]. The human body is complex and heterogeneous with different tissues, all of which have unique dielectric properties.

Specifically, the dielectric properties of tissues are frequency- and tissue-dependent. Tissues of higher water content such as muscle and cerebral spinal fluid are more conductive than dryer or oily tissues such as bone and fat, and some tissues such as bone and nerve tissues have elongated cells and can be anisotropic. There is also substantial variation in the measured properties within a given organ, as a function of age, and across individuals and species [169], [170].

There is a wide range of measured data on tissue properties [74]. The most commonly-used data for healthy tissues is [171]. Data is also available for many types of cancerous tissues, as well. When homogeneous models are used, for quick approximation of whole-body exposures to far-field sources, it is standard to use 2/3 muscle for the tissue properties. This means the permittivity and conductivity are each multiplied by 2/3. More recent data includes the variability and uncertainty of the measurements [171], which results in variation in electromagnetic dosimetry results [172], [173].

2) EXPERIMENTAL EVALUATION

Tissue mimicking phantoms have been designed and characterized in several studies [174]–[178]. The core ingredient varies with each phantom causing the material to acquire three different forms: liquid, solid, and semi-solid. Most liquid phantoms are composed of water and saline mixtures since the human body is mostly water. These phantoms have been used in several applications testing wearable and implantable antenna and RF components [174]–[178]. Although easy to develop, liquid phantoms cannot be used to emulate complex tissues where the testing is done using multiple layers of tissues such as skin/muscle/fat composition. In addition, liquid phantoms lose their initial electrical properties due to evaporation and the environmental conditions they are kept in. For these reasons, the most popular and easy to use phantoms are made of solid or semi-solid materials. In addition, testing the device in liquids can be messy and quite cumbersome. The solid phantoms synthesized in previous research consisted of plastics, polyethylene powder and saline, silicon rubber, ceramic powder and resin, and strontium titanite powder and resin [33], [179]–[185]. Solid body phantoms have longer shelf life, are easier to handle and test. However, they are not suitable for SAR measurements where the access inside the phantom is required [33], [183]–[187]. The solid phantoms are mainly constructed using the average dielectric properties among various tissues rather than of each individual tissue. As a result, phantoms with multiple layers of tissue cannot be synthesized. To tackle this issue, semi-solid phantoms are introduced that utilize various materials as described in [188]–[204], Fig. 7.

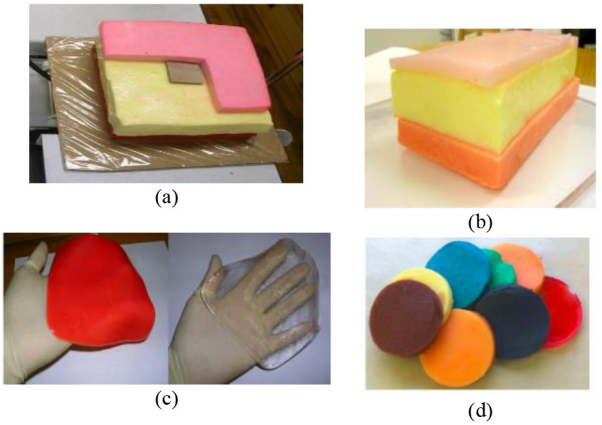

FIGURE 7. (a) Implantable Antenna testing using 3-layer muscle-fat-skin gel, (b) Construction of complex tissues using layered gels, (c) Adjustable gel thickness and color using different formulas in [192]-[196] (d) Gels mimicking various tissues including Kidney, Pancreas, Brain, Liver, Tumor, Fat, Muscle and Skin.

Whether liquid, solid or semi-solid all phantoms tend to enable reasonable performance evaluation in terms of efficiency and radiation patterns. At higher frequencies (e.g., above 6 GHz), the EM waves do not penetrate deeply into the body and hence the internal structure is less critical. At lower frequencies, wearable antennas will be affected by the muscle and bone below the skin and the fat. Therefore, these semi-solid phantoms are more suitable for lower frequencies.

For example, semi-solid layered (skin-fat-muscle) phantoms were developed at 950 MHz band [205] and at 20 MHz band [206]. Semi-solid phantoms are suitable to the experiments for implantable antennas, in particular, because it is quite easy to embed antennas at the right position in the phantoms and to fix them without any additional support.

Another example of semi-solid phantoms is a so-called "UWB phantom" [207]. A single phantom is required for the evaluation of UWB antennas over the entire wide frequency range. By adjusting its composition properly, the UWB phantom [207] covers the frequency range from 2 GHz to 10 GHz. Other publications utilizing semi-solid and solid phantoms consider also more sophisticated heterogenous phantoms. These phantoms are suitable for applications that require the representation of heterogeneous tissues and organs. For instance, depending on the frequency of operation, one approach is to use effective electrical properties of a specific tissue like skin at low frequencies, while at higher frequencies, the layers of the skin need to be individually fabricated to better mimic the overall electrical properties which semi-solid and solid phantoms offer a good solution.

Although there are many ways to measure the electrical properties of phantoms, the most commonly used technique is to utilize an open-ended coaxial cable that allows the measurement of dielectric constant and conductivity for a wide variety of frequencies [39], [176], [177], [193]. These reflection coefficient-based measurements allow the properties of interest to be measured from 50 MHz to 50 GHz covering the majority of microwave frequency bands. This is

extremely important since mm-wave 5G deployment, which covers 26-28 GHz bands and above, is in the near horizon. This next generation of mm-wave 5G will require the deployment of more antennas, transmitters, and receivers which will increase the need for research on human body – mm-wave interaction. Besides implantable and wearable applications, the development of high-frequency tissue mimicking phantoms will play a crucial role for the study of these interactions.

There are many challenges to human-body physical phantoms such as a dynamic phantom and a transparent phantom, to just name a few. A dynamic phantom is needed to simulate movement of the human body or internal blood flow. If a semi-solid phantom is transparent, it would be easy to locate implantable antennas and to confirm their conditions from outside of the phantom. In addition, every human has a different shape of head and different composition of tissues. It is important to carry out electromagnetic simulations with the different available anatomical models which account for age (e.g., adults vs. children) and other inter-subject variability [208].

Overall, the phantom development for medical applications continues to evolve as 3D printing technologies improve. We anticipate that, in the near future, more realistic personalized human body phantoms will become a reality.

3) COMPUTATIONAL EVALUATION

1) Models of the body and sources: There are numerous models of the body at various levels of detail. Simple models such as prolate spheroids [209], simple block models [210], and layered models [211] that were commonly used throughout the 1970s-1990s are surprisingly good at estimating the total field exposure in the body due to a plane wave, and can be used for quick estimates. Simple models may also be useful for very near-field applications, where the fields do not reach other parts of the body, and hence, they have little or no effect. To predict detailed distributions of the fields in and around the body from near-field sources more detailed anatomical models are used.

Anatomical models based on Magnetic Resonance Imaging (MRI) or Computed Tomography (CT) scans or X-rays/visual images, are often used for both nuclear radiation and bioelectromagnetic dosimetry [212]. These include the GSF family of models (adults, children, infants) [143], [212], the Yale Voxelman [213], [214], NORMAN man model [215], [216] and NAOMI woman model [217], RPI VIP Man [218], [219], the Utah Man Model [220], [221] and Utah Head Model [211], the Visible Man and Woman project from the National Institutes of Health [222], Japanese Computational Phantoms that include adults, children, infants, and pregnant women at various stages of gestation [223], voxel [224] and polygonal [225] male and female models based on CT scans, Korean adult models [226], [227], pregnant models in different positions [228]. An example SAR distribution generated by an implanted antenna within five different head models (two canonical/spherical and three anatomical) is shown in Fig. 8. Indeed, high resolution models of specific parts of the body such as the head [229], heart, lungs, thorax [230], [231], breast [232], [233] are available. Models of mice and rats, crabs, fish, frogs, dogs, bees, deer, ducks, worms, goats, pigs, and rabbits also exist [229], [234]. When the electromagnetic effects are highly localized, as with many near-field sources, only the impacted portions of the model need to be used, thus saving computational time.

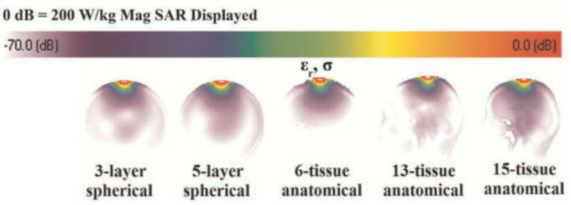

FIGURE 8. Distribution of the 1-g averaged SAR generated by an implanted antenna inside five head models [239].

Specific details of the model can make a profound difference on the fields produced in and around the body. Height [235], size (e.g., adult vs. child, size of head, torso, or other parts of the body) [236], shape, tissue properties, etc. all impact the fields. Even individual portions of the body such as the head have their own size-dependent resonances [237]. Here, we note that challenges with creating good anatomical models for electromagnetic dosimetry include a shift in the apparent location of fat and water-based tissues such as muscle by as much as 4-5mm in MR-derived images [211], deflation of the lungs, heart, and other organs when deceased bodies are modeled [30], changes in shape from models lying prone (such as feet resting in a toes-pointed position rather than flat) [220], blur or jitter from moving organs such as beating heart and breathing lungs, and a general difficulty in characterizing the material in regions between major organs [220].

For electromagnetic sources that are in or very near the body (medical implants, cell phones, wearables, etc.) the exact placement and orientation of the source significantly impacts the field distribution [172], [238]. Near-field sources such as cell phones, medical implants, etc., require great precision in their modeling. X-rays [221] and CAD models have been used to provide detailed modeling [239]. How the source is placed in/near the body also has a significant impact on the fields [172], [236]. Far-field sources typically require somewhat less precision.

2) Computational methods: Computational methods use approximations of electromagnetic wave propagation to determine how the fields propagate from internal and/or external sources and reflect, propagate, and absorb within the voxel models of the body as described earlier in Section II-D3 (with each voxel having defined tissue properties). The fields can be approximated in either the frequency domain (as with the impedance method, method of moments [240], or finite-element method (FEM) [240]) or in the time

domain using the finite-difference time-domain (FDTD) method [241] or finite element time domain method [242]. In the frequency domain the fields are treated as being sinusoidal steady state, where any transient effects have died away. The magnitude and phase of the sinusoidal field is calculated in each voxel in the model. In the time domain the transient fields are calculated in each voxel as a function of time.

The FDTD method is widely used in bioelectromagnetics due to its efficiency and versatility. It has been used to model fields in the human body with high resolution (1 mm or less) for a wide variety of sources from 60 Hz [243] through optical frequencies [241]. FDTD solves the time domain Maxwell's equations for the six vector components of the electric and magnetic fields in a voxel model of the body. The voxel size (Δ) is most often chosen based on the size of the physical structure being evaluated. This then determines the maximum frequency for that model, as Δ should be $< \lambda_{min}/10$. The FDTD method has been extended to very low frequency simulations (down to 60 Hz) [243], broad band models where the electrical properties of the tissues vary with frequency [244], and models where the electrical [173], [245] and geometric [246] properties of the tissues vary statistically.

4) DOSIMETRY

Bioelectromagnetic dosimetry predicts the dose and nature (polarization, frequency spectrum, etc.) of electromagnetic fields in the body. It is important for device design, evaluation of the interaction between electromagnetic sources and the body, and understanding or controlling the natural electric fields of the body. This can be done with either simulations or measurements [247]. The application of interest controls whether the dosimetry is needed in the frequency domain, time domain, or both, and it is common to transform between these two domains. The application also controls the frequency band of interest. Broad-band measurements and simulations can be difficult. It is generally more efficient to simulate single frequencies and combine them for broader band applications. The bandwidth of measurements can also be limited by how well-matched tissue simulant materials can be to real tissues over broad bands, and the accuracy of measurement equipment over broad bands. For both simulations and measurements, it is common to evaluate individual frequencies or narrower bands, and combine them computationally as needed.

Numerical dosimetry requires: (1) an appropriate model of the body and the electromagnetic source, (2) dielectric properties of the tissues and materials at the frequencies of interest, and (3) a computational method that can simulate the electromagnetic fields. Each of these have been discussed earlier in Section II-D. Experimental dosimetry requires (1) an appropriate phantom model of the body, including materials with appropriate materials to represent the body tissues at the frequencies of interest, (2) an appropriate electromagnetic source, (3) a measurement method that can measure the electromagnetic fields without significantly perturbing them. The first two of these were discussed in Section II-D, and the measurement methods are discussed below.

Specific absorption rate (SAR) is a widely-used dosimetric measure, due to its use in regulations and guidelines [248]. With a semi-solid phantom, two-dimensional SAR distribution can be quickly evaluated by use of the thermographic method [249]. This technique utilizes measured temperature rise on the phantom surface caused by short-time EM exposure. The SAR on the observation plane is figured by the following equation:

$$SAR = c \cdot \Delta T / \Delta t [W/kg] \tag{1}$$

where c is the specific heat of the phantom, ΔT is the temperature rise, and Δt is the EM exposure time. When the exposure time is short enough, the above equation gives reasonable results. Another advantage this method is that it can be easily applied to a system with multiple frequencies or wide spectrum, because it is independent of frequency.

SAR is also measured by using electric field probes to measure the electric field E, and then calculating it from:

$$SAR = \frac{\sigma |E|^2}{2\rho} \quad \left[W/kg\right] \tag{2}$$

where σ is the electrical conductivity [S/m), and ρ is the tissue density $[kg/m^3]$. SAR is typically averaged over 1-gram or 10-gram sections of tissue, and today's guidelines require inclusion of a variation budget to account for expected variability in the models and measurements [250], [251].

III. EMERGING BIOELECTROMAGNETICS APPLICATIONS

A. MICROWAVE ABLATION

Therapeutic applications of microwave energy include ablation, diathermy and hyperthermia. These techniques are often called as thermal therapies, which basically employ temperature elevation in human tissue. Unlike hyperthermia that is usually required to heat the tumor up to the temperature between 42 and 45 $^{\circ}C$, ablation heats up the tumor/tissue over 60 °C. Microwave Ablation (MWA) utilizes a thin antenna or an applicator which is inserted directly into the target tissue to be treated [16]. Typical operating frequencies are 915 MHz and 2.45 GHz. Fig. 9 shows some examples of typical antennas for MWA. In Fig. 9(c), a quarter-wavelength sleeve is attached to suppress the electric currents flowing back on the outer conductor as described later in this section. Coaxial-slot antennas [252] shown in Fig. 9(d) and (e) have been widely employed for clinical use.

Recently, with the advent of various medical imaging technologies and an increasing demand for improving QOL (quality of life) of patients, image-guided MWA has emerged as a minimally invasive therapeutic modality for the treatment of unresectable tumors and cardiac arrhythmias, neuromodulation, and other applications. One of the key techniques to MWA is how to guide an antenna to the

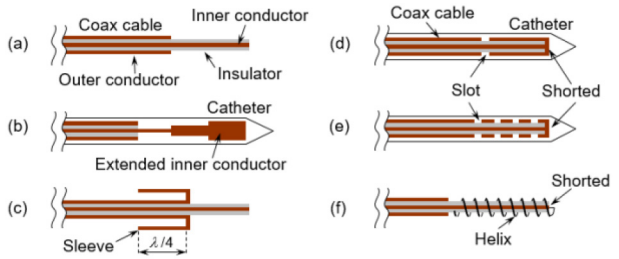

FIGURE 9. Examples of typical antennas for MWA: (a) Monopole antenna, (b) Extended monopole antenna, (c) Sleeve antenna, (d) Coaxial-slot antenna [252], (e) Coaxial-slot antenna with multiple slots [252], (f) Helical antenna.

right position for treatment. MWA has been widely performed under the guidance of computed tomography (CT). Alternatively, ultrasound (US) has been used as the guidance to avoid exposure to ionizing radiation and to reduce the cost [253]. However, for these imaging techniques, image contrast may be sometimes insufficient and therefore treatment may not be perfect. More recently, magnetic resonance (MR) guidance has been developed as a promising modality, although the cost is rather high [254].

In terms of electromagnetic ablation, besides MWA, RFA (Radio Frequency Ablation) and LA (Laser Ablation) have been widely applied to clinical use. RFA has two different systems, namely, monopolar and bipolar systems. Typical operating frequency range for RFA is about 400 kHz to 500 kHz. A monopolar RFA system requires an external electrode to form an electric current path. Both MWA and RFA have advantages and disadvantages in clinical treatment. Comparison between MWA and RFA has been discussed and summarized in, for example, [255] and [256] from clinical viewpoint. LA is another type of minimally invasive therapeutic modality using the laser light and an optical fiber [257]. MR-guided LA is an option for the treatment of brain tumors, in particular. It may further reduce certain risks associated with traditional open brain surgery.

Antennas used in MWA systems should ensure efficient power transfer to the targeted tissue, through a heating pattern well matched to the size and shape of the target. Most MWA antennas generate axisymmetric heating patterns around the antennas in homogenous tissue because of their axisymmetric structure. However, a directional heating pattern may be required for some specific scenarios where, for example, a target tumor is close to the bowel which should not be ablated. Different types of MWA antennas with directional heating patterns have been developed and reported [258]–[260].

Most MWA antennas are made of thin coaxial cables and designed with some mechanism to suppress the electric currents flowing back on the outer surface of the coaxial cables. These outer-surface electric currents may cause unwanted heating of healthy tissue along the antennas. Different techniques have been proposed to control or localize heating patterns along the antennas. For conventional coaxial-slot antennas [252], the number of slots or slot positions have been changed to control heating patterns to some degree. Another way is to attach a tapered slot balun which achieved localized heating patterns and good impedance matching over a wide frequency range [261].

Traditionally, RF current or ultrasonic vibration have been widely applied to surgical devices for cutting or coagulating biological tissues during surgery. However, they have some drawbacks such as generating unwanted excessive high temperature or creating mist and spray [262]. Recently, microwave energy has been successfully applied to modern surgical devices which are necessary for laparoscopic surgery [262], [263].

There are still many challenges to microwave ablation. In this section, two important challenges are addressed. Specifically, it is essential for the development of MWA antennas and clinical treatment planning to numerically evaluate distributions of SAR as well as temperature in tissues generated by the antennas. For such numerical evaluation, biological tissues are modelled with their physical properties including dielectric and thermal parameters. Unlike hyperthermia, a significant change of dielectric and thermal parameters must be considered during ablation treatment, because the targeted tissue gets desiccated or charred with temperature well exceeding 60 °C. It is obvious that the water content ratio over the targeted tissue significantly affects physical properties of the tissue. Several groups have studied and reported numerical modelling and experimental validation of microwave ablation incorporating water vaporization or dehydration [264], [265]. For further improvement, other factors such as a change of blood flow rate and tissue contraction should be incorporated as well.

The term “theranostics” is used as a combination of “therapeutics” and “diagnostics” that are combined simultaneously or sequentially in a clinical situation. For example, a compact and thin microwave theranostic device was developed and reported in [266] which can act as an applicator for thermal ablation and as a sensor to detect malignant tissue. The device employs oval-shaped Split Ring Resonators (SRRs) working in a frequency range between 8 GHz and 12 GHz. In the treatment mode, SRRs perform microwave ablation. For the detection mode, resonance frequency changes due to abnormalities are evaluated. Although further work should be done to realize such theranostic devices, they would be quite beneficial not only to hospitals but also to patients.

B. MICROWAVE IMAGING

Microwave imaging for biomedical applications has a long history. It started with the idea of extending to diffracted radiation (at radiofrequencies and microwaves) the diagnostic approaches originally based on ray propagation. Microwave imaging aims at providing qualitative or quantitative maps of the dielectric properties of the body under test (e.g., dielectric permittivity and electric conductivity), correlating them with the presence of any pathology. Indeed, implementing this imaging modality needs to face several problems

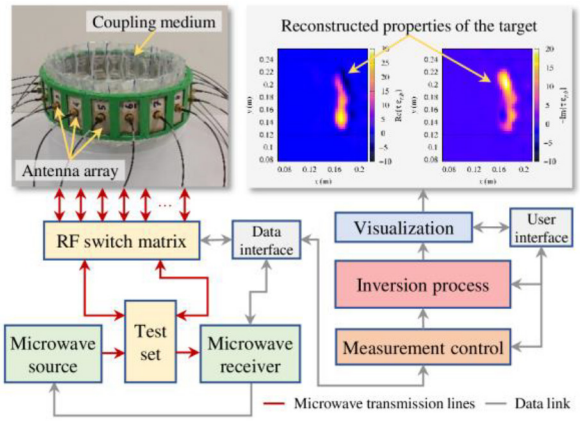

FIGURE 10. Configuration and main components of a microwave imaging system for biomedical applications.

and challenges, which mainly derive from scattering and polarization effects of microwave radiation.

The pioneering results in this field, collected by Larsen and Jacobi [267], were achieved around 40 years ago. Compared to the historical developments of other techniques (e.g., X-ray computerized tomography and magnetic resonance imaging), a spontaneous question raises concerning the real-life potential of microwave imaging as an effective tool for medical diagnostics. Indeed, despite a sequence of "enthusiastic" and "disillusion" phases throughout the years (as very well explained in [268]) this challenging problem is nowadays tackled by a continuously increasing number of research teams around the world and new optimistic perspectives seem to be opened by many recent developments.

The typical configuration of a biomedical microwave imaging system is illustrated in Fig. 10, which shows its main components and an example of results. Roughly, two essential parts are identified: the microwave measurement system (on the left) and the control/processing techniques (on the right). The measurement system aims at collecting, in the most accurate way, measures of the electromagnetic field or some related quantities (e.g., transmission/reflection S-parameters) around the body under test. This is done by means of a set of custom antenna elements. A coupling medium (liquid or solid) is usually interposed between those imaging antennas and body, but discussions exist on its relevance and its composition, which also depend on the proposed application. The acquired data are exploited to solve a radar-based, statistical or an inverse scattering problem, whose solution technique can be seen as the "core" of the whole imaging methodology. The inversion process is theoretically nonlinear if no simplifying approximations are assumed [269].

All these components require special care if medical diagnostics are pursued. Limiting factors may arise due to the possibly low dielectric contrast between tissues of interest, the achievable spatial resolution, as well as the difficulty of developing suitable reconstruction algorithms. The recent improvements towards these issues have been thoroughly discussed in several books (see, for example, [269]–[271] and the references therein), which delineate microwave imaging methods as complementary tools with respect to more consolidated diagnostic techniques.

One of the first proposed applications for medical imaging at microwave frequencies is related to the detection of breast tumors. Despite the conflicting studies about the dielectric characterization of breast tissues and the scarcity of *in vivo* measured data, several systems have been developed with the goal of performing clinical trials. Recent results have been summarized and compared in some detailed review papers, such as [272]. Some systems are close to enter in a commercialization phase. As to the inversion process, there is a large variety of proposed methodologies, such as those based on tomography, radar-based approaches, and microwave holography. Both quantitative [273] and qualitative methods [274]–[276] have been proposed and applied to experimental systems, with pros and cons not always so simple to understand with respect to the real disease to be detected. It is worth noting that portable and wearable imaging devices have also been designed and initially validated in clinical settings. Although most systems operate between 1 and 10 GHz, recent research aims at checking the possible diagnosis of breast tumors at higher frequencies.

Another field where microwave-based diagnostics have recently shown promising outcomes is the detection of brain stroke. In particular, along with the devices that aim at an early stroke classification [277], other approaches investigate the quantitative reconstruction of the internal dielectric properties of brain [278], [279]. Qualitative and hybrid imaging modalities have also been considered, also assessing the possible use of flexible antenna arrays [280]. Head scanning systems for stroke imaging are currently undergoing clinical trials with encouraging results [281], [282].

In addition, other medical applications are currently pioneered by the research community. For instance, the detection of osteoporosis has been initially investigated some years ago and is now seeing a renewed interest [283]. Another application is the imaging of the chest [284], which may be interesting for detecting the fluid accumulation inside and around lungs. Furthermore, portable microwave systems for knee imaging have been recently proposed [285], also developed as a wearable textile brace [286], with the goal of detecting ligaments/tendon tears. Microwave imaging of the neck has also been considered, for the possible diagnosis of cervical diseases [287]. Moreover, recent studies propose the use of imaging techniques at microwave frequencies for the monitoring of thermal ablation (which is discussed in another section).

In summary, while novel clinical uses of microwave imaging are currently under investigation, such interesting perspectives require systematic analyses from both theoretical and experimental points of view. It is worth noting that, in the validation of experimental imaging systems, a key role is

played by the development of suitable phantoms of the body region of interest [288]. Of course, a better knowledge of the contrast in the dielectric properties of healthy and pathological tissues *in vivo* is crucial. Considering the impressive increase in the available computing power, as well as the continuous improvements in microwave and antenna technologies needed to develop effective imaging apparatuses, a major challenge is still represented by processing and reconstruction methods, which – despite a plethora of proposals and tests – need further works and comparisons.

C. NEUROSENSING

1) NEUROSENSING APPLICATIONS AND NEURAL SIGNALS

The ability to record brain signals has the potential to improve the understanding and treatment of a variety of neurologically based conditions including Alzheimer's, epilepsy, depression, addiction, and more [289]–[291]. However, current brain-computer interface (BCI) technology falls short of fulfilling such potential due to safety concerns, which limit the recording environment and increase patient risk. These concerns include: (1) wired connections from the implant to the external environment, which restricts recording to a laboratory setting [291], [292]; (2) reliance on batteries, which require additional surgeries for replacement [293]; and (3) densely packed electronics on the implant, which can generate enough heat to damage surrounding neurons [294].

To address these shortcomings, wireless passive neural implants were proposed [93], [111]. These passive neurosensors operate much like a RFID tag, utilizing an external interrogator to transmit a signal to turn on an implant, which then transmits the neural signals back to the interrogator where post-processing can occur. Given the low voltage of neural signals (down to 2 or 20 μV_{pp}), many of these implants still require power, typically via power harvesting, to amplify neural signals before transmission to the interrogator. Another class of BCIs, so-called wireless fully passive neurosensors, relies solely on microwave backscattering for transmitting the modulated signal, thus eliminating the need for power at the implant. Both passive and fully passive devices address the concerns with traditional BCIs, but likewise come with their own challenges.

2) PASSIVE NEUROSENSORS

Passive devices utilize an energy harvester on the implant to amplify low-level neural signals prior to transmitting to the interrogator. Unlike traditional BCIs, passive devices do not store energy and therefore do not require a battery. The most successful source from which to harvest the power thus far is inductive power transfer, but harvesting the body's glucose is also being explored [111]. For inductive power transfer, the wireless link in combination with an integrated circuit (IC) on the implant serves to rectify and regulate the power provided for amplification. Thus, wireless link optimization is key for passive sensing.

Given the use of inductive coupling, various versions of external and implanted loop antenna systems operating in the frequency range of a few hundred MHz to a few GHz are used for the wireless link [111], [295]. For the interrogator, the primary goals are minimizing specific absorption rate (SAR) while maximizing power transfer. To reduce "hotspots" on the loop antenna and therefore SAR of the tissue below, [296], [297] divided a loop antenna into two segments connected by capacitors, while [111] suggests tilting the interrogator to be nonparallel to the tissue below. Increasing the number of loops also helps maximize power transfer [298].

Though these passive devices eliminate the need for wired connections and batteries, they still use an IC, which requires space and power. The addition of an IC increases the size of a 1 mm^3 implant by at least 100%, increasing the likelihood of initiating the body's immune response to a foreign object [299]. Transmitting power to the implant poses a risk in terms of tissue heating, and thus, SAR must be carefully considered in the system design. Additionally, these loop antennas are sensitive to misalignment, which is almost a guarantee given the antennas cannot be visually aligned.

3) FULLY PASSIVE NEUROSENSORS

To eliminate the need for an implanted IC, fully passive neurosensors rely on microwave backscattering and perform all amplification at the interrogator. The interrogator transmits a carrier signal, which is then mixed by the implant with neural signals prior to backscattering a higher order mixing product (i.e., second harmonic) to the interrogator for demodulation. Fully passive devices typically operate on the order of a few GHz, most with a 2.4 GHz carrier signal and a backscattered mixing product centered at 4.8 GHz. The higher frequencies equate to smaller and more complex antenna designs than the loops used for passive devices, but tissue attenuation limits the upper frequency and therefore antenna size.

In [300], a 10×3.5 mm^2 implant using a slot antenna with a diode pair and chip capacitor to perform the fully passive mixing communicated with a waveguide antenna interrogator as a proof-of-concept. Building on the proof-of-concept, [301], [302] use a slot antenna for both antennas and detects 6 mVpp emulated neural signals from a function generator with the antennas transmitting through a skin and bone phantom. Aiming to improve sensitivity, [303] use an anti-parallel diode pair for the mixer, an E-shaped patch antenna for the implant, and a spiral for the interrogator. The sensor detects function generator emulated neural signals as low as 63 μVpp through a 2/3-muscle phantom [35]. To reduce the size of the implant from 39×15 mm^2 to 8.7×10 mm^2, the implant is folded in half with the circuit on one side, the antenna on the other, and the ground plane sandwiched between, and a higher permittivity substrate is used. Sensitivity is increased to 20 μVpp by optimizing the implant matching network and using a patch antenna for the interrogator [304], [305].

Challenges with fully passive devices center around the lack of power at the implant. In fact, the conductivity of tissues is typically high, and it thus dissipates the interrogated power into heat. Hence, the overall power available at the implant might not be adequate to operate the system considering the amount of absorbed power by head tissues.

Neural electrodes typically have very high, frequency-dependent impedances (tens of kΩ to MΩ), which traditional BCIs match with operating amplifiers [299], but this technique requires power. In [18], a bipolar junction transistor (BJT) passively increases the implant impedance but is only able to match lower impedance electrodes (i.e., macro instead of microelectrodes) [306]. Additionally, the discussed passive and fully passive devices are limited to recording a single channel (i.e., one electrode, one brain location). In [307], [308], multichannel devices using photodiodes for channel switching are designed but the devices are large (40×40 mm^2), can only record from 8 channels, and cannot concurrently record channels. As with passive devices, antenna misalignment is also an issue [309], as is biocompatibility of the implant [299].

D. NEUROSTIMULATION

Electric and magnetic stimulation of neural tissues, such as transcranial magnetic stimulation and deep brain stimulation, are widely adopted in neuroengineering as an attempt to restore partial neural function, usually lost due to disease or traumatic injury. An increasing number of medical conditions are being treated with neurostimulators, and have resulted in encouraging, and sometimes dramatic, partial restoration of function [310]. The premise for these implants generally involves injecting current through electrodes to directly stimulate downstream neurons, thus bypassing the upstream diseased or damaged neural circuitry. Computational and experimental bioelectromagnetics methods are at the core of the development of modern neurostimulators, which are now complex systems integrating multifunctional capabilities (such as recording, sensing, and stimulating) [258], [259], wireless devices (for efficient wireless power and data transcutaneous transmission) [312]–[314] and biocompatible interfaces and packaging. The ultimate and ambitious goal is to render neurostimulators "true" biomimetic systems, capable to replacing the lost functionality of damaged neurons in a seamless way, with safe and selective neuroactivation of downstream neurons, in small form factors that are compatible with surgical interventions. Although the complexity deriving from the multi-temporal and multi-spatial natures of the nervous system - spanning multiple disciplines from large-scale electromagnetic field and thermal modeling to neuromodeling - has hindered the rapid progression in this field, recent advances in computational and experimental bioelectromagnetics embrace this complexity and open new doors to potential treatments.

Low frequency bioelectromagnetics is considered particularly significant for neurostimulation applications, owing to both the very low frequency content of neural signals and the traditional low frequency embodiment of wireless power and data transfer systems. Of particular relevance to the development of modern neurostimulators is the newly acquired capability to model electromagnetic signaling in complex, large, morphologically accurate, neural networks [315]–[318]. "Connectomics" – as it is commonly referred to – provides comprehensive, morphologically accurate maps of the neural network [316]; the ability to handle Terabyte-sized connective maps of both healthy and degenerated/diseased neural networks enables an unprecedented opportunity to understand signaling at the network level, and consequently design neurostimulators through bioelectromagnetic predictive modeling methods. Further, innovation in multi-coil wireless systems and metasurfaces has opened the opportunity to realize wireless neuroimplants that are smaller and more efficient than ever before [7], [319]–[323].

Several neuroimplants capture the innovation described above. Examples of these systems are an artificial retina to restore partial vision to the blind [324], [325] and a hippocampal prosthetic for memory restoration [318]. The artificial retina attempts to restore vision in the blind affected by progressive and relentlessly advancing retinal degeneration conditions, such as Retinitis Pigmentosa (RP) and Age-Related Macular Degeneration (AMD). There is no known cure for these conditions; in these pathologies, photoreceptors (the neural cells converting light to electrical signal) progressively degenerate, ultimately resulting in further neuronal damage, functional alterations, and extensive remodeling of retinal networks. Over the past 25 years, researchers have been working on a device comprised of an epiretinal electrode array to directly stimulate surviving retinal cells and supporting system to drive such array, including a camera to record images in front of the patient and a wireless system to transfer power and image data to the implanted device. The design of the epiretinal electrode array and stimulating waveforms – designed to target retinal cells with specificity while avoiding undesirable effects such as direct stimulation of axon or spontaneous firing of retinal cells – can be successfully carried out with the use of low-frequency computational platforms supported by pathoconnectomes of the retina (Fig. 11). These pathoconnectomes (connectomes of the diseased retina at various stages of degeneration), when utilized with low-frequency electromagnetic computational methods, have allowed for the development of neurostimulation signals that have greatly improved the opportunity in retinal prosthetic, such as the ability to encode "color" in the percept [315] or avoid the direct stimulation of axons, thus avoid "streaking" vision percepts. Integration with Computer Vision and Artificial Intelligence methods enables improvement of image interpretation and understanding (e.g., object recognition) as well as image processing tasks (e.g., segmentation) and opens up new opportunities towards the development of novel task-based visual assistive systems [326], [327].

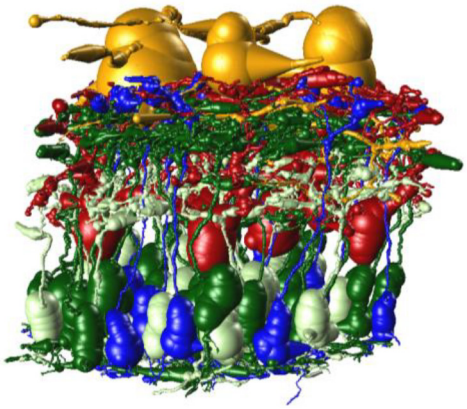

FIGURE 11. Model of the pathoconnectome of the first stage degenerated retina tiled with elements of a healthy connectome to create a complete retinal network. Accurate electrical models of the neural cells in this network, as well as the capability to model extremely large computational networks, has enabled the opportunity to accurately predict neural response in a diseased neural network as a result of neurostimulation. Figure courtesy of Dr. P. Kosta, University of Southern California. Data from the laboratory of Dr. B. Jones, the University of Utah.

IV. CONCLUSION

This paper provided a comprehensive overview of enabling technologies for next-generation wearables and implants and illuminated some key applications of high clinical promise. As is evident, opportunities brought forward by electromagnetics in healthcare are exciting. It is, thus, not surprising that extensive research is currently being pursued in this regard and that numerous wearables and implants are being commercialized and employed in applications as diverse as healthcare, sports, defense, consumer electronics, and more.

As would be expected, a number of challenges still remain to be resolved. Body area antennas need to overcome losses associated with the tissue environment; wearables need to be made more reliable, secure, and seamlessly embedded in day-to-day garments; implants need to be further miniaturized without compromising performance; efficiency of RF power harvesting needs to be improved; inductive links should be made more reliable and robust to misalignment; flexible conductors and inks need to be formulated with conductivity close to copper while still being biocompatible; phantoms should account for the frequency-dependent properties of tissues and maintain these properties over the course of time; patient safety must be ensured at all times and numerical/experimental evaluations should be optimized to match real-world scenarios; high data rate transmissions need to be enabled; minimally invasive technologies should replace traditional surgically-implanted devices; additive manufacturing technologies should be optimized for environmentally-friendly solutions, fast prototyping and 3D complex structures; theranostic devices for microwave ablation need to be refined for clinical applications; microwave imaging technologies should achieve higher resolution than currently possible; neurosensors should be made wireless and batteryless; neurostimulators should be empowered with multifunctional capabilities (such as recording, sensing, and stimulating).

The abovementioned list of challenges is by no means limiting and research opportunities in electromagnetics, antennas, dosimetry, sensors, electronics, and materials are truly endless.

REFERENCES

[1] P. Momenroodaki, W. Haines, M. Fromandi, and Z. Popovic, "Noninvasive internal body temperature tracking with near-field microwave radiometry," *IEEE Trans. Microw. Theory Techn.*, vol. 66, no. 5, pp. 2535–2545, May 2018.

[2] G. Lazzi, R. Lee, and K. S. Nikita, "Guest editorial for the special issue on wireless real-time health monitoring technology for personalized medicine," *IEEE Trans. Antennas Propag.*, vol. 67, no. 8, pp. 4946–4954, Aug. 2019.

[3] A. Kiourti and K. S. Nikita, "A review of in-body biotelemetry devices: Implantables, ingestibles, and injectables," *IEEE Trans. Biomed. Eng.*, vol. 64, no. 7, pp. 1422–1430, Jul. 2017.

[4] S. Ma, L. Sydänheimo, L. Ukkonen, and T. Björninen, "Split-ring resonator antenna system with cortical implant and head-worn parts for effective far-field implant communications," *IEEE Antennas Wireless Propag. Lett.*, vol. 17, pp. 710–713, 2018.

[5] A. Kiourti and K. S. Nikita, "A review of implantable patch antennas for biomedical telemetry: Challenges and solutions," *IEEE Antennas Propag. Mag.*, vol. 54, no. 3, pp. 210–228, Jun. 2012.

[6] P. Rayner, S. Zhang, D. Cadman, J. Vardaxoglou, and W. Whittow, "Wearable and meshed wideband monopole antennas and their interactions with the human body," *IET Microw. Antennas Propag.*, vol. 13, no. 14, pp. 2412–2418, 2019.

[7] M. Machnoor, J. Paknahad, J. Stang, and G. Lazzi, "Wireless telemetry system with independent power and data frequency resonance," *IEEE Antennas Wireless Propag. Lett.*, vol. 19, pp. 690–694, 2020.

[8] M. Manoufali, K. Bialkowski, B. Mohammed, and A. Abbosh, "Wireless power link based on inductive coupling for brain implantable medical devices," *IEEE Antennas Wireless Propag. Lett.*, vol. 17, pp. 160–163, 2018.

[9] A. Eid *et al.*, "Nanotechnology-empowered flexible printed wireless electronics: A review of various applications of printed materials," *IEEE Nanotechnol. Mag.*, vol. 13, no. 1, pp. 18–29, Feb. 2019.

[10] A. Eid *et al.*, "Inkjet-/3D-/4D-printed perpetual electronics and modules: RF and mm-wave devices for 5G+, IoT, smart agriculture, and smart cities applications," *IEEE Microw. Mag.*, vol. 21, no. 12, pp. 87–103, Dec. 2020.

[11] A. Kiourti, "RFID antennas for body-area applications: From wearables to implants," *IEEE Antennas Propag. Mag.*, vol. 60, no. 5, pp. 14–25, Oct. 2018.

[12] F. Curry, A. M. Chrysler, T. Tasnim, J. E. Shea, C. M. Furse, and H. Zhang, "Biostable conductive nanocomposite for implantable subdermal antenna," *APL Mater.*, vol. 8, Oct. 2020, Art. no. 101112.

[13] T. Karacolak, A. Z. Hood, and E. Topsakal, "Design of a dual-band implantable antenna and development of skin mimicking gels for continuous glucose monitoring," *IEEE Trans. Microw. Theory Techn.*, vol. 56, no. 4, pp. 1001–1008, Apr. 2008.

[14] K. Guido, C. Matos, J. Ramsey, and A. Kiourti, "Tissue-emulating phantoms for in vitro experimentation at radio frequencies: Exploring characteristics, fabrication, and testing methods," *IEEE Antennas Propag. Mag.*, vol. 63, no. 6, pp. 29–39, Dec. 2021.

[15] *IEC/IEEE International Standard—Determining the Peak Spatial-Average Specific Absorption Rate (SAR) in the Human Body From Wireless Communications Devices, 30 MHz to 6 GHz—Part 1: General Requirements for Using the Finite-Difference Time-Domain (FDTD)*, IEC/IEEE Standard 62704-1:2017, 2017, pp. 1–86.

[16] K. Saito and K. Ito, "Preliminary investigation of numerical estimation of coagulated region generated by interstitial microwave antenna," *Int. J. Hyperth.*, vol. 33, no. 1, pp. 69–73, 2017.

[17] A. Fedeli, C. Estatico, M. Pastorino, and A. Randazzo, "Microwave detection of brain injuries by means of a hybrid imaging method," *IEEE Open J. Antennas Propag.*, vol. 1, pp. 513–523, 2020.

[18] W.-C. Chen, K. Guido, and A. Kiourti, "Passive impedance matching for implanted brain–electrode interfaces," *IEEE J. Electromagn., RF, Microw. Med. Biol.*, vol. 3, no. 4, pp. 233–239, Dec. 2019.

[19] P. Kosta, J. Mize, D. J. Warren, and G. Lazzi, "Simulation-based optimization of figure-of-eight coil designs and orientations for magnetic stimulation of peripheral nerve," *IEEE Trans. Neural Syst. Rehabil. Eng.*, vol. 28, no. 12, pp. 2901–2913, Dec. 2020.

[20] Y. Rahmat-Samii and E. Topsakal, *Antenna and Sensor Technologies in Modern Medical Applications*. Hoboken, NJ, USA: Wiley, 2021.

[21] A. Kiourti, J. R. Costa, C. A. Fernandes, and K. S. Nikita, "A broadband implantable and a dual-band on-body repeater antenna: Design and transmission performance," *IEEE Trans. Antennas Propag.*, vol. 62, no. 6, pp. 2899–2908, Jun. 2014.

[22] S. Zhu and R. Langley, "Dual-band wearable textile antenna on an EBG substrate," *IEEE Trans. Antennas Propag.*, vol. 57, no. 4, pp. 926–935, Apr. 2009.

[23] I. Locher, M. Klemm, T. Kirstein, and G. Tröster, "Design and characterization of purely textile patch antennas," *IEEE Trans. Adv. Packag.*, vol. 29, no. 4, pp. 777–788, Nov. 2006.

[24] C. Hertleer, H. Rogier, L. Vallozzi, and L. Van Langenhove, "A textile antenna for off-body communication integrated into protective clothing for firefighters," *IEEE Trans. Antennas Propag.*, vol. 57, no. 4, pp. 919–925, Apr. 2009.

[25] D. P. Rose *et al.*, "Adhesive RFID sensor patch for monitoring of sweat electrolytes," *IEEE Trans. Biomed. Eng.*, vol. 62, no. 6, pp. 1457–1465, Jun. 2015.

[26] H. R. Raad, A. I. Abbosh, H. M. Al-Rizzo, and D. G. Rucker, "Flexible and compact AMC based antenna for telemedicine applications," *IEEE Trans. Antennas Propag.*, vol. 61, no. 2, pp. 524–531, Feb. 2013.

[27] G. A. Conway and W. G. Scanlon, "Antennas for over-body-surface communication at 2.45 GHz," *IEEE Trans. Antennas Propag.*, vol. 57, no. 4, pp. 844–855, Apr. 2009.

[28] Z. H. Jiang, D. E. Brocker, P. E. Sieber, and D. H. Werner, "A compact, low-profile metasurface-enabled antenna for wearable medical body-area network devices," *IEEE Trans. Antennas Propag.*, vol. 62, no. 8, pp. 4021–4030, Aug. 2014.

[29] A. Kiourti and J. L. Volakis, *Wearable Antennas and Electronics*. Boston, MA, USA: Artech House, 2022.

[30] A. Kiourti, C. Lee, and J. L. Volakis, "Fabrication of textile antennas and circuits with 0.1 mm precision," *IEEE Antennas Wireless Propag. Lett.*, vol. 15, pp. 151–153, 2015.

[31] A. Kiourti and J. L. Volakis, "High-geometrical-accuracy embroidery process for textile antennas with fine details," *IEEE Antennas Wireless Propag. Lett.*, vol. 14, pp. 1474–1477, 2014.

[32] A. Kiourti and J. L. Volakis, "Stretchable and flexible E-fiber wire antennas embedded in polymer," *IEEE Antennas Wireless Propag. Lett.*, vol. 13, pp. 1381–1384, 2014.

[33] S. Zhang, A. Paraskevopoulos, C. Luxey, J. Pinto, and W. Whittow, "Broad-band embroidered spiral antenna for off-body communications," *IET Microw. Antennas Propag.*, vol. 10, no. 13, pp. 1395–1401, 2016.

[34] "Evaluating compliance with FCC guidelines for human exposure to radio frequency electromagnetic fields," OET Bull. FCC, Washington, DC, USA, document OET Bulletin 65, 1997. [Online]. Available: https://www.fcc.gov/general/oet-bulletins-line

[35] J. Nagel, C. Furse, D. A. Christensen, and C. H. Durney, *Basic Introduction to Bioelectromagnetics*, 3rd ed. Boca Raton, FL, USA: CRC Press, 2009.

[36] J. Andreu-Perez, D. R. Leff, H. M. D. Ip, and G.-Z. Yang, "From wearable sensors to smart implants—Toward pervasive and personalized healthcare," *IEEE Trans. Biomed. Eng.*, vol. 62, no. 12, pp. 2750–2761, Dec. 2015.

[37] J. M. Rabaey, "Towards TRUE human-centric computation," *Comput. Commun.*, vol. 131, pp. 73–76, Oct. 2018.

[38] A. Kiourti and K. S. Nikita, "Recent advances in implantable antennas for medical telemetry," *IEEE Antennas Propag. Mag.*, vol. 54, no. 6, pp. 190–199, Dec. 2012.

[39] A. Kiourti, J. R. Costa, C. A. Fernandes, A. G. Santiago, and K. S. Nikita, "Miniature implantable antennas for biomedical telemetry: From simulation to realization," *IEEE Trans. Biomed. Eng.*, vol. 59, no. 11, pp. 3140–3147, Nov. 2012.

[40] S. Gabriel, R. W. Lau, and C. Gabriel, "The dielectric properties of biological tissues: III. Parametric models for the dielectric spectrum of tissues," *Phys. Med. Biol.*, vol. 41, no. 11, pp. 2271–2293, 1996.

[41] M. Zaiembashi *et al.*, "NanoNeuroRFID: A wireless implantable device based on magnetoelectric antennas," *IEEE J. Electromagn., RF, Microw. Med. Biol.*, vol. 3, no. 3, pp. 206–215, Sep. 2019.

[42] A. Kiourti and K. S. Nikita, "Miniature scalp-implantable antennas for telemetry in the MICS and ISM bands: Design, safety considerations and link budget analysis," *IEEE Trans. Antennas Propag.*, vol. 60, no. 6, pp. 3568–3575, Aug. 2012.

[43] D. Nikolayev, M. Zhadobov, P. Karban, and R. Sauleau, "Electromagnetic radiation efficiency of body-implanted devices," *Phys. Rev. Appl.*, vol. 9, no. 2, p. 12, 2018.

[44] M. Gao, D. Nikolayev, M. Bosiljevac, Z. Šipuš, and A. K. Skrivervik, "Rules of thumb to assess losses of implanted antennas," in *Proc. Eur. Conf. Antennas Propag.*, vol. 5, 2021, pp. 1–5.

[45] Y. El-Saboni, D. E. Zelenchuk, G. A. Conway, and W. G. Scanlon, "Assessing the intrinsic radiation efficiency of tissue-implanted UHF antennas," *IEEE Trans. Antennas Propag.*, vol. 68, no. 1, pp. 491–499, Jan. 2020.

[46] Z. Bao, Y.-X. Guo, and R. Mittra, "An ultrawideband conformal capsule antenna with stable impedance matching," *IEEE Trans. Antennas Propag.*, vol. 65, no. 10, pp. 5086–5094, Oct. 2017.

[47] L. Luo, B. Hu, J. Wu, T. Yan, and L.-J. Xu, "Compact dual-band antenna with slotted ground for implantable applications," *Microw. Opt. Technol. Lett.*, vol. 61, no. 5, pp. 1314–1319, 2019.

[48] F. Faisal and H. Yoo, "A miniaturized novel-shape dual-band antenna for implantable applications," *IEEE Trans. Antennas Propag.*, vol. 67, no. 2, pp. 774–783, Feb. 2019.

[49] S. Bakogianni and S. Koulouridis, "A dual-band implantable rectenna for wireless data and power support at sub-GHZ region," *IEEE Trans. Antennas Propag.*, vol. 67, no. 11, pp. 6800–6810, Nov. 2019.

[50] F. Faisal, M. Zada, A. Ejaz, Y. Amin, S. Ullah, and H. Yoo, "A miniaturized dual-band implantable antenna system for medical applications," *IEEE Trans. Antennas Propag.*, vol. 68, no. 2, pp. 1161–1165, Feb. 2020.

[51] S. Ding, S. Koulouridis, and L. Pichon, "Design and characterization of a dual-band miniaturized circular antenna for deep in body biomedical wireless applications," *Intl. J. Microw. Wireless Technol.*, vol. 12, no. 6, pp. 461–468, 2020.

[52] I. A. Shah, M. Zada, and H. Yoo, "Design and analysis of a compact-sized multiband spiral-shaped implantable antenna for scalp implantable and leadless pacemaker systems," *IEEE Trans. Antennas Propag.*, vol. 67, no. 6, pp. 4230–4234, Jun. 2019.

[53] T.-A. L. Trong, S. I. H. Shah, G. Shin, S. M. Radha, and I.-J. Yoon, "A compact triple-band antenna with a broadside radiation characteristic for head-implantable wireless communications," *IEEE Antennas Wireless Propag. Lett.*, vol. 20, pp. 958–962, 2021.

[54] J. Shang, Y. Yu, and L.-J. Xu, "Compact dual-band implantable planar inverted-F antenna with bandwidth enhancement," *Microw. Opt. Technol. Lett.*, vol. 62, no. 1, pp. 322–328, 2020.

[55] A. Basir, A. Bouazizi, M. Zada, A. Iqbal, S. Ullah, and U. Naeem, "A dual-band implantable antenna with wide-band characteristics at MICS and ISM bands," *Microw. Opt. Technol. Lett.*, vol. 60, no. 12, pp. 2944–2949, 2018.

[56] Z. Jiang *et al.*, "Wideband loop antenna with split-ring resonators for wireless medical telemetry," *IEEE Trans. Antennas Wireless Propag. Lett.*, vol. 18, pp. 1415–1419, 2019.

[57] C. Liu, Y.-X. Guo, and S. Xiao, "Capacitively loaded circularly polarized implantable patch antenna for ISM band biomedical applications," *IEEE Trans. Antennas Propag.*, vol. 62, no. 5, pp. 2407–2417, May 2014.

[58] C. Liu, Y. Zhang, and X. Liu, "Circularly polarized implantable antenna for 915 MHz ISM-band far-field wireless power transmission," *IEEE Antennas Wireless Propag. Lett.*, vol. 17, pp. 373–376, 2018.

[59] Y. Zhang, C. Liu, X. Liu, K. Zhang, and X. Yang, "A wideband circularly polarized implantable antenna for 915 MHz ISM-band biotelemetry devices," *IEEE Antennas Wireless Propag. Lett.*, vol. 17, pp. 1473–1477, 2018.

[60] G. Samanta and D. Mitra, "Dual-band circular polarized flexible implantable antenna using reactive impedance substrate," *IEEE Trans. Antennas Propag.*, vol. 67, no. 6, pp. 4218–4223, Jun. 2019.

[61] M. Zada, I. A. Shah, and H. Yoo, "Metamaterial-loaded compact high-gain dual-band circularly polarized implantable antenna system for multiple biomedical applications," *IEEE Trans. Antennas Propag.*, vol. 68, no. 2, pp. 1140–1144, Feb. 2020.

[62] S. Hayat, S. A. A. Shah, and H. Yoo, "Miniaturized dual-band circularly polarized implantable antenna for capsule endoscopic system," *IEEE Trans. Antennas Propag.*, vol. 69, no. 4, pp. 1885–1895, Apr. 2021.

[63] Z. Xia *et al.*, "A wideband circularly polarized implantable patch antenna for ISM band biomedical applications," *IEEE Trans. Antennas Propag.*, vol. 68, no. 3, pp. 2399–2404, Mar. 2020.

[64] R. Liu *et al.*, "A wideband circular polarization implantable antenna for health monitor microsystem," *IEEE Antennas Wireless Propag. Lett.*, vol. 20, pp. 848–852, 2021.

[65] L.-J. Xu, J.-P. Xu, Z.-J. Chu, S. Liu, and X. Zhu, "Circularly polarized implantable antenna with improved impedance matching," *IEEE Antennas Wireless Propag. Lett.*, vol. 19, pp. 876–880, 2020.

[66] R. Muller *et al.*, "A minimally invasive 64-channel wireless μECoG implant," *IEEE J. Solid-State Circuits*, vol. 50, no. 1, pp. 344–359, Jan. 2015.

[67] S. Ma, L. Sydänheimo, L. Ukkonen, and T. Björninen, "Robustness evaluation of split ring resonator antenna system for wireless brain care in semi-anatomical ellipsoid head model," *Appl. Comput. Electromagn. Soc. J.*, vol. 33, no. 9, pp. 966–972, 2018.

[68] S. Ma, T. Björninen, L. Sydänheimo, M. H. Voutilainen, and L. Ukkonen, "Double split rings as extremely small and tuneable antennas for brain implantable wireless medical microsystems," *IEEE Trans. Antennas Propag.*, vol. 69, no. 2, pp. 760–768, Feb. 2021.

[69] M. Ghovanloo and M. Kiani, "Inductive coupling," in *Handbook of Biomedical Telemetry*. Hoboken, NJ, USA: Wiley, 2014.

[70] E. Romero, *Powering Biomedical Devices*. Boston, MA, USA: Academic, 2013.

[71] A. K. Teshome, B. Kibret, and D. T. H. Lai, "A review of implant communication technology in WBAN: Progress and challenges," *IEEE Rev. Biomed. Eng.*, vol. 12, pp. 88–99, Jun. 2018.

[72] M. Haerinia and R. Shadid, "Wireless power transfer approaches for medical implants: A review," *Signals*, vol. 1, no. 2, pp. 209–229, 2020.

[73] H.-J. Kim, H. Hirayama, S. Kim, K. J. Han, R. Zhang, and J.-W. Choi, "Review of near-field wireless power and communication for biomedical applications," *IEEE Access*, vol. 5, pp. 21264–21285, 2017.

[74] C. Gabriel, S. Gabriel, and E. Corthout, "The dielectric properties of biological tissues: I literature survey," *Phys. Med. Biol.*, vol. 41, no. 11, pp. 2231–2249, 1996.

[75] J. M. Elloian, G. M. Noetscher, S. N. Makarov, and A. Pascual-Leone, "Continuous wave simulations on the propagation of electromagnetic fields through the human head," *IEEE Trans. Biomed. Eng.*, vol. 61, no. 6, pp. 1676–1683, Jun. 2014.

[76] A. Ferikoğlu, O. Çerezci, M. Kahriman, and S. Ç. Yener, "Electromagnetic absorption rate in a multilayer human tissue model exposed to base-station radiation using transmission line analysis," *IEEE Antennas Wireless Propag. Lett.*, vol. 13, pp. 903–906, 2014.

[77] R. Lodato, V. Lopresto, R. Pinto, and G. Marrocco, "Numerical and experimental characterization of through-the-body UHF-RFID links for passive tags implanted into human limbs," *IEEE Trans. Antennas Propag.*, vol. 62, no. 10, pp. 5298–5306, Oct. 2014.

[78] S. R. Khan, S. K. Pavuluri, G. Cummins, and M. P. Y. Desmulliez, "Wireless power transfer techniques for implantable medical devices: A review," *Sensors*, vol. 20, no. 12, pp. 1–58, 2020.

[79] M. Schormans, V. Valente, and A. Demosthenous, "Practical inductive link design for biomedical wireless power transfer: A tutorial," *IEEE Trans. Biomed. Circuits Syst.*, vol. 12, no. 5, pp. 1112–1130, Oct. 2018.

[80] M. Mark *et al.*, "Wireless channel characterization for mm-size neural implants," in *Proc. Annu. Int. Conf. IEEE Eng. Med. Biol. Conf.*, 2010, pp. 1565–1568.

[81] R. Sarpeshkar, *Ultra Low Power Bioelectronics. Fundamentals, Biomedical Applications, and Bio-Inspired Systems*. Cambridge, U.K.: Cambridge Univ. Press, 2010.

[82] A. Sani, M. Rajab, R. Foster, and Y. Hao, "Antennas and propagation of implanted RFIDs for pervasive healthcare applications," *Proc. IEEE*, vol. 98, no. 9, pp. 1648–1655, Sep. 2010.

[83] M. J. Karimi, A. Schmid, and C. Dehollain, "Wireless power and data transmission for implanted devices via inductive links: A systematic review," *IEEE Sensors J.*, vol. 21, no. 6, pp. 7145–7161, Mar. 2021.

[84] A. K. RamRakhyani, S. Mirabbasi, and M. Chiao, "Design and optimization of resonance-based efficient wireless power delivery systems for biomedical implants," *IEEE Trans. Biomed. Circuits Syst.*, vol. 5, no. 1, pp. 48–63, Feb. 2011.

[85] W. Liu *et al.*, "Implantable biomimetic microelectronic systems design," *IEEE Eng. Med. Biol. Mag.*, vol. 24, no. 5, pp. 66–74, Sep./Oct. 2005.

[86] H. Ali, T. J. Ahmad, and S. A. Khan, "Inductive link design for medical implants," in *Proc. IEEE Symp. Ind. Electron. Appl.*, 2009, pp. 694–699.

[87] M. Ghovanloo and S. Atluri, "A wide-band power-efficient inductive wireless link for implantable microelectronic devices using multiple carriers," *IEEE Trans. Circuits Syst. I, Reg. Papers*, vol. 54, no. 10, pp. 2211–2221, Oct. 2007.

[88] A. Yakovlev, S. Kim, and A. Poon, "Implantable biomedical devices: Wireless powering and communication," *IEEE Commun. Mag.*, vol. 50, no. 4, pp. 152–159, Apr. 2012.

[89] M. A. Hannan, S. M. Abbas, S. A. Samad, and A. Hussain, "Modulation techniques for biomedical implanted devices and their challenges," *Sensors*, vol. 12, no. 1, pp. 297–319, 2012.

[90] A. S. Y. Poon, S. O. Driscoll, and T. H. Meng, "Optimal frequency for wireless power transmission into dispersive tissue," *IEEE Trans. Antennas Propag.*, vol. 58, no. 5, pp. 1739–1750, May 2010.

[91] D. Pivonka, A. Yakovlev, A. S. Y. Poon, and T. Meng, "A mm-sized wirelessly powered and remotely controlled locomotive implant," *IEEE Trans. Biomed. Circuits Syst.*, vol. 6, no. 6, pp. 523–532, Dec. 2012.

[92] S. Amendola *et al.*, "Design and optimization of mm-size implantable and wearable on-body antennas for biomedical systems," in *Proc. 8th Eur. Conf. Antennas Propag. (EuCAP)*, 2014, pp. 520–524.

[93] L. Song and Y. Rahmat-Samii, "An end-to-end implanted brain–machine interface antenna system performance characterizations and development," *IEEE Trans. Antennas Propag.*, vol. 65, no. 7, pp. 3399–3408, Jul. 2017.

[94] M. Manoufali, K. Bialkowski, B. J. Mohammad, P. C. Mills, and A. Abbosh, "Near-field inductive-coupling link to power a three-dimensional millimeter-size antenna for brain implantable medical devices," *IEEE Trans. Biomed. Eng.*, vol. 65, no. 1, pp. 4–14, Jan. 2018.

[95] A. Ibrahim and M. Kiani, "A figure-of-merit for design and optimization of inductive power transmission links for millimeter-sized biomedical implants," *IEEE Trans. Biomed. Circuits Syst.*, vol. 10, no. 6, pp. 1100–1111, Dec. 2016.

[96] D. Ahn and M. Ghovanloo, "Optimal design of wireless power transmission links for millimeter-sized biomedical implants," *IEEE Trans. Biomed. Circuits Syst.*, vol. 10, no. 1, pp. 125–137, Feb. 2016.

[97] H. Rahmani and A. Babakhani, "A dual-mode RF power harvesting system with an on-chip coil in 180-nm SOI CMOS for millimeter-sized biomedical implants," *IEEE Trans. Microw. Theory Techn.*, vol. 67, no. 1, pp. 414–428, Jan. 2019.

[98] G. Monti, P. Arcuti, and L. Tarricone, "Resonant inductive link for remote powering of pacemakers," *IEEE Trans. Microw. Theory Techn.*, vol. 63, no. 11, pp. 3814–3822, Nov. 2015.

[99] L. Li, H. Liu, H. Zhang, and W. Xue, "Efficient wireless power transfer system integrating with metasurface for biological application," *IEEE Trans. Ind. Electron.*, vol. 65, no. 4, pp. 3230–3239, Apr. 2018.

[100] N. A. Quadir, L. Albasha, M. Taghadosi, N. Qaddoumi, and B. Hatahet, "Low-power implanted sensor for orthodontic bond failure diagnosis and detection," *IEEE Sensors J.*, vol. 18, no. 7, pp. 3003–3009, Apr. 2018.

[101] E. Moradi *et al.*, "Backscattering neural tags for wireless brain-machine interface systems," *IEEE Trans. Antennas Propag.*, vol. 63, no. 2, pp. 719–726, Feb. 2015.

[102] A. B. Amar, A. B. Kouki, and H. Cao, "Power approaches for implantable medical devices," *Sensors*, vol. 15, pp. 28889–28914, Nov. 2015.

[103] K. Agarwal, R. Jegadeesan, Y.-X. Guo, and N. V. Thakor, "Wireless power transfer strategies for implantable bioelectronics," *IEEE Rev. Biomed. Eng.*, vol. 10, no. 99, pp. 136–161, Mar. 2017.

[104] A. Khaleghi, A. Hasanvand, and I. Balasingham, "Radio frequency backscatter communication for high data rate deep implants," *IEEE Trans. Microw. Theory Techn.*, vol. 67, no. 3, pp. 1093–1106, Mar. 2019.

[105] N. Vidal and J. M. López-Villegas, "Changes in electromagnetic field absorption in the presence of subcutaneous implanted devices: Minimizing increases in absorption," *IEEE Trans. Electromagn. Compat.*, vol. 52, no. 3, pp. 545–555, Aug. 2010.

[106] S. Gabriel, R. W. Lau, and C. Gabriel, "The dielectric properties of biological tissues: II. Measurements in the frequency range 10 Hz to 20 GHz," *Phys. Med. Biol.*, vol. 41, no. 11, pp. 2251–2269, 1996.

[107] M. Manoufali, S. A. R. Naqvi, and A. M. Abbosh, "Accurate Fourth-order debye model for the head tissues across the 0.1–1 GHz band using metaheuristic genetic algorithm," *IEEE J. Electromagn., RF, Microw. Med. Biol.*, vol. 2, no. 2, pp. 79–86, Jun. 2018.

[108] M. Kiani and M. Ghovanloo, "The circuit theory behind coupled-mode magnetic resonance-based wireless power transmission," *IEEE Trans. Circuits Syst. I, Reg. Papers*, vol. 59, no. 9, pp. 2065–2074, Sep. 2012.

[109] Y. El-Saboni, M. K. Magill, G. A. Conway, S. L. Cotton, and W. G. Scanlon, "Measurement of deep tissue implanted antenna efficiency using a reverberation chamber," *IEEE J. Electromagn., RF, Microw. Med. Biol.*, vol. 1, no. 2, pp. 90–97, Dec. 2017.

[110] J. S. Ho, S. Kim, and A. S. Y. Poon, "Midfield wireless powering for implantable systems," *Proc. IEEE*, vol. 101, no. 6, pp. 1369–1378, Jun. 2013.

[111] S. Rao *et al.*, "Miniature implantable and wearable on-body antennas: Towards the new era of wireless body-centric systems [antenna applications corner]," *IEEE Antennas Propag. Mag.*, vol. 56, no. 1, pp. 271–291, Feb. 2014.

[112] F. Lu, H. Zhang, and C. Mi, "A review on the recent development of capacitive wireless power transfer technology," *Energies*, vol. 10, no. 11, pp. 1–30, 2017.

[113] A. I. Al-Kalbani, M. R. Yuce, and J.-M. Redouté, "A biosafety comparison between capacitive and inductive coupling in biomedical implants," *IEEE Antennas Wireless Propag. Lett.*, vol. 13, pp. 1168–1171, 2014.

[114] R. Jegadeesan, K. Agarwal, Y.-X. Guo, S.-C. Yen, and N. V. Thakor, "Wireless power delivery to flexible subcutaneous implants using capacitive coupling," *IEEE Trans. Microw. Theory Techn.*, vol. 65, no. 1, pp. 280–292, Jan. 2017.

[115] A. K. Teshome, B. Kibret, and D. T. H. Lai, "Galvanically coupled intrabody communications for medical implants: A unified analytic model," *IEEE Trans. Antennas Propag.*, vol. 64, no. 7, pp. 2989–3002, Jul. 2016.

[116] M. Manoufali, K. Bialkowski, A. T. Mobashsher, B. Mohammed, and A. Abbosh, "In situ near-field path loss and data communication link for brain implantable medical devices using software-defined radio," *IEEE Trans. Antennas Propag.*, vol. 68, no. 9, pp. 6787–6799, Sep. 2020.

[117] C. Liu, Y.-X. Guo, H. Sun, and S. Xiao, "Design and safety considerations of an implantable rectenna for far-field wireless power transfer," *IEEE Trans. Antennas Propag.*, vol. 62, no. 11, pp. 5798–5806, Nov. 2014.

[118] A. Tsolis, W. G. Whittow, A. A. Alexandridis, and J. C. Vardaxoglou, "Embroidery and related manufacturing techniques for wearable antennas: Challenges and opportunities," *Electronics*, vol. 3, no. 2, pp. 314–338, 2014.

[119] C. Hertleer, H. R. Van Laere, H. Rogier, and L. V. Langenhove, "Influence of relative humidity on textile antenna performance," *Text. Res. J.*, vol. 80, no. 2, pp. 177–183, 2009.

[120] M. A. R. Osman, M. K. A. Rahim, N. A. Samsuri, M. K. Elbasheer, and M. E. Ali, "Textile UWB antenna bending and wet performances," *Int. J. Antennas Propag.*, vol. 2012, pp. 1–12, May 2012.

[121] T. Acti *et al.*, "Embroidered wire dipole antennas using novel copper yarns," *IEEE Antennas Propag. Wireless Lett.*, vol. 14, pp. 638–641, 2015.

[122] R. D. Seager *et al.*, "Effect of the fabrication parameters on the performance of embroidered antennas," *IET Microw. Antennas Propag.*, vol. 7, no. 14, pp. 1174–1181, 2013.

[123] Z. Wang, L. Zhang, Y. Bayram, and J. L. Volakis, "Embroidered conductive fibers on polymer composite for conformal antennas," *IEEE Trans. Antennas Propag.*, vol. 60, no. 9, pp. 4141–4147, Sep. 2012.

[124] Z. Wang, L. Z. Lee, D. Psychoudakis, and J. L. Volakis, "Embroidered multiband body-worn antenna for GSM/PCS/WLAN communications," *IEEE Trans. Antennas Propag.*, vol. 62, no. 6, pp. 3321–3329, Jun. 2014.

[125] "NORA DELL." Hitek. [Online]. Available: https://www.hitek-ltd.co.uk/product-page/nora-dell (Accessed: Feb. 24, 2022).

[126] A. Chauraya *et al.*, "Inkjet printed dipole antennas on textiles for wearable communications," *IET Microw. Antennas Propag.*, vol. 7, no. 9, pp. 760–767, 2013.

[127] W. G. Whittow *et al.*, "Inkjet-printed microstrip patch antennas realized on textile for wearable applications," *IEEE Antennas Wireless Propag. Lett.*, vol. 13, pp. 71–74, 2014.

[128] V. P. S. Neto, C. F. L. Vasconcelos, M. R. M. L. Albuquerque, and A. G. Dassuncao, "Study of annular ring patch antennas on anisotropic substrates by WCIP method," in *Proc. 9th Eur. Conf. Antennas Propag. (EuCAP)*, 2015, pp. 1–4.

[129] C. S. Gurel and E. Yazgan, "Characteristics of a circular patch microstrip antenna on uniaxially anisotropic substrate," *IEEE Trans. Antennas Propag.*, vol. 52, no. 10, pp. 2532–2537, Oct. 2004.

[130] S. M. Yang and C.-C. Hung, "Modal analysis of microstrip antenna on fiber reinforced anisotropic substrates," *IEEE Trans. Antennas Propag.*, vol. 57, no. 3, pp. 792–796, Mar. 2009.

[131] P. I. Dankov, V. P. Levcheva, and P. K. Sharma, "Influence of dielectric anisotropy and bending on wearable textile antenna properties," in *Proc. Int. Workshop Antenna Technol. (iWAT)*, 2020, pp. 1–4.

[132] T. Tuovinen, M. Berg, and E. T. Salonen, "Antenna close to tissue: Avoiding radiation pattern minima with an anisotropic substrate," *IEEE Antennas Wireless Propag. Lett.*, vol. 13, pp. 1680–1683, 2014.

[133] A. Y. I. Ashyap *et al.*, "Compact and low-profile textile EBG-based antenna for wearable medical applications," *IEEE Antennas Wireless Propag. Lett.*, vol. 16, pp. 2550–2553, 2017.

[134] A. Y. I. Ashyap *et al.*, "Robust and efficient integrated antenna with EBG-DGS enabled wide bandwidth for wearable medical device applications," *IEEE Access*, vol. 8, pp. 56346–56358, 2020.

[135] A. Iqbal *et al.*, "Electromagnetic bandgap backed millimeter-wave MIMO antenna for wearable applications," *IEEE Access*, vol. 7, pp. 111135–111144, 2019.

[136] J. Joubert, J. C. Vardaxoglou, W. G. Whittow, and J. W. Odendaal, "CPW-fed cavity-backed slot radiator loaded with an AMC reflector," *IEEE Trans. Antennas Propag.*, vol. 60, no. 2, pp. 735–742, Feb. 2012.

[137] S. Genovesi, F. Costa, F. Fanciulli, and A. Monorchio, "Wearable inkjet-printed wideband antenna by using miniaturized AMC for sub-GHz applications," *IEEE Antennas Wireless Propag. Lett.*, vol. 15, pp. 1927–1930, 2016.

[138] S. Genovesi, I. R. Butterworth, J. E. C. Serrallés, and L. Daniel, "Metasurface matching layers for enhanced electric field penetration into the human body," *IEEE Access*, vol. 8, pp. 197745–197756, 2020.

[139] A. Y. I. Ashyap *et al.*, "An overview of electromagnetic band-gap integrated wearable antennas," *IEEE Access*, vol. 8, pp. 7641–7658, 2020.

[140] C. D. Suriyakala and A. Eldhose, "Meta surface enabled wearable antenna for medical implant applications," in *Proc. Int. Conf. Circuit Power Comput. Technol. (ICCPCT)*, 2017, pp. 1–6.

[141] X. Liu, Y. Di, H. Liu, Z. Wu, and M. M. Tentzeris, "A planar windmill-like broadband antenna equipped with artificial magnetic conductor for off-body communications," *IEEE Antennas Wireless Propag. Lett.*, vol. 15, pp. 64–67, 2016.

[142] A. Chrysler, K. Hall, F. Curry, Jr., and H. Zhang, "Effect of conductivity on subdermal antennas," *Microw. Opt. Technol. Lett.*, vol. 60, no. 5, pp. 1154–1160, 2018.

[143] N. Petoussi-Henss, M. Zankl, U. Fill, and D. Regulla, "The GSF family of voxel phantoms," *Phys. Med. Biol.*, vol. 47, no. 1, pp. 89–106, 2002.

[144] H. Zhang, "Graph theoretical design of biomimetic aramid nanofiber composites as insulation coatings for implantable bioelectronics," *MRS Bull.*, vol. 46, pp. 576–587, Apr. 2021.

[145] J. P. Seymour, Y. M. Elkasabi, H.-Y. Chen, J. Lahann, and D. R. Kipke, "The insulation performance of reactive parylene films in implantable electronic devices," *Biomaterials*, vol. 30, no. 31, pp. 6158–6167, 2009.

[146] S.-W. Hwang, "A physically transient form of silicon electronics," *Science*, vol. 337, no. 6102, pp. 1640–1644, 2012.

[147] Q. Zheng, "Biodegradable triboelectric nanogenerator as a life-time designed implantable power source," *Sci. Adv.*, vol. 2, no. 3, 2016, Art. no. 1501478.

[148] K. K. Fu, Z. Wang, J. Dai, M. Carter, and L. Hu, "Transient electronics: Materials and devices," *Chem. Mater.*, vol. 28, no. 11, pp. 3527–3539, 2016.

[149] C. M. Boutry, H. Chandrahalim, P. Streit, M. Schinhammer, A. C. Hänzi, and C. Hierold, "Towards biodegradable wireless implants," *Philos. Trans. Roy. Soc. A, Math. Phys. Eng. Sci.*, vol. 370, pp. 2418–2432, May 2012.

[150] D. R. Merrill, "Materials considerations of implantable neuroengineering devices for clinical use," *Current Opinion Solid-State Mater. Sci.*, vol. 18, no. 6, pp. 329–336, 2014.

[151] F. Curry, Jr. *et al.*, "Biostable conductive nanocomposite for subdermal antenna," *APL Mater.*, vol. 8, no. 10, 2020, Art. no. 101112.

[152] D.-H. Kim *et al.*, "Epidermal electronics," *Science*, vol. 333, no. 6044, pp. 838–843, 2011.

[153] E. B. Malarkey and V. Parpura, "Applications of carbon nanotubes in neurobiology," *Neuro Degener. Dis.*, vol. 4, no. 4, pp. 292–299, 2007. [Online]. Available: https://search.proquest.com/docview/1069369026?fromopenview=true&pq-origsite=gscholar

[154] E. K. Wujcik and C. N. Monty, "Nanotechnology for implantable sensors: Carbon nanotubes and graphene in medicine," *WIREs Nanomed. Nanobiotechnol.*, vol. 5, no. 3, pp. 233–249, 2013.

[155] A. Moscicki, J. Felba, T. Sobierajski, J. Kudzia, A. Arp, and W. Meyer, "Electrically conductive formulations filled nano size silver filler for ink-jet technology," in *Proc. 5th Int. Conf. Polym. Adhesives Microelectron. Photon.*, 2005, pp. 40–44.

[156] J. Sidén, M. Fein, A. Koptyug, and H.-E. Nilsson, "Printed antennas with variable conductive ink layer thickness," *IET Microw. Antennas Propag.*, vol. 1, no. 2, pp. 401–407, 2007.

[157] M. A. Gaynes, R. H. Lewis, R. F. Saraf, and J. M. Roldan, "Evaluation of contact resistance for isotropic electrically conductive adhesives," *IEEE Trans. Compon. Packag. Manuf. Technol. B*, vol. 18, no. 2, pp. 299–304, May 1995.

[158] K. Bock, "Polytronics—Electronics and systems on flexible substrates," in *Proc. IEEE VLSI-TSA Int. Symp. VLSI Technol. (VLSI-TSA-Tech)*, 2005, pp. 53–56.

[159] A. R. Duggal and L. M. Levinson, "A novel high current density switching effect in electrically conductive polymer composite materials," *J. Appl. Phys.*, vol. 82, no. 11, pp. 5532–5539, 1997.

[160] "NovaCentrix." [Online]. Available: https://www.novacentrix.com/ (Accessed: Jan. 2, 2022).

[161] M. D. Dickey, "Emerging applications of liquid metals featuring surface oxides," *ACS Appl. Mater. Interfaces*, vol. 6, no. 21, pp. 18369–18379, 2014.

[162] R. Vasold, E. Engel, B. König, M. Landthaler, and W. Bäumler, "Health risks of tattoo colors," *Anal. Bioanal. Chem.*, vol. 391, no. 1, pp. 9–13, 2008.

[163] E. C. Cho, Q. Zhang, and Y. Xia, "The effect of sedimentation and diffusion on cellular uptake of gold nanoparticles," *Nat. Nanotechnol.*, vol. 6, no. 6, pp. 385–391, 2011.

[164] A. Eid, J. G. Hester, and M. M. Tentzeris, "5G as a wireless power grid," *Sci. Rep.*, vol. 11, no. 1, pp. 1–9, 2021.

[165] A. Eid, J. G. D. Hester, and M. M. Tentzeris, "Rotman lens-based wide angular coverage and high-gain semipassive architecture for ultralong range mm-wave RFIDs," *IEEE Antennas Wireless Propag. Lett.*, vol. 19, pp. 1943–1947, 2020.

[166] J. G. D. Hester and M. M. Tentzeris, "Inkjet-printed flexible mm-wave Van-Atta reflectarrays: A solution for ultralong-range dense multitag and multisensing chipless RFID implementations for IoT smart skins," *IEEE Trans. Microw. Theory Techn.*, vol. 64, no. 12, pp. 4763–4773, Dec. 2016.

[167] S. A. Nauroze and M. M. Tentzeris, "A thermally actuated fully inkjet-printed origami-inspired multilayer frequency selective surface with continuous-range tunability using polyester-based substrates," *IEEE Trans. Microw. Theory Techn.*, vol. 67, no. 12, pp. 4944–4954, Dec. 2019.

[168] X. He, B. K. Tehrani, R. Bahr, W. Su, and M. M. Tentzeris, "Additively manufactured mm-wave multichip modules with fully printed 'smart' encapsulation structures," *IEEE Trans. Microw. Theory Techn.*, vol. 68, no. 7, pp. 2716–2724, Jul. 2020.

[169] C. Gabriel, "Dielectric properties of biological tissue: Variation with age," *Bioelectromagnetics*, vol. 26, no. S7, pp. 12–18, 2005.

[170] C. Gabriel and A. Peyman, "Dielectric measurement: Error analysis and assessment of uncertainty," *Phys. Med. Biol.*, vol. 51, no. 23, pp. 6033–6046, 2006.

[171] C. Gabriel, "Compilation of the dielectric properties of body tissues at RF and microwave frequencies," in *Occupational and Environmental Health Directorate Radiofrequency Radiation Division*. San Antonio, TX, USA: Brooks Airforce Base, 1996.

[172] J. D. Johnson, "Statistical analysis of detuning effects for implantable microstrip antennas," M.S. thesis, Dept. Electr. Comput. Eng., Univ. Utah, Salt Lake City, UT, USA, 2007.

[173] S. M. Smith and C. Furse, "Stochastic FDTD for analysis of statistical variation in electromagnetic fields," *IEEE Trans. Antennas Propag.*, vol. 60, no. 7, pp. 3343–3350, Jul. 2012.

[174] M. Y. Ballen, M. Y. Kanda, C.-K. Chou, and Q. Balzano, "Formulation and characterization of tissue simulating liquids used for SAR measurement," in *Proc. 23rd Annu. Bioelectromagn. Soc. Meeting*, vol. 14, p. 80, 2001.

[175] A. Peyman and C. Gabriel, "Tissue equivalent liquids for SAR measurement at microwave frequencies," in *Proc. 24th Annu. Bioelectromagn. Soc. Meeting*, 2002, pp. 184–185.

[176] K. Fukunaga, S. Watanabe, and Y. Yamanaka, "Dielectric properties of tissue-equivalent liquids and their effects on specific absorption rate," *IEEE Trans. Electromagn. Compat.*, vol. 46, no. 1, pp. 126–129, Feb. 2004.

[177] K. Fukunaga, S. Watanabe, H. Asou, and K. Sato, "Dielectric properties of non-toxic tissue-equivalent liquids for radiowave safety tests," in *Proc. IEEE Int. Conf. Dielectr. Liquids*, 2005, pp. 425–428.

[178] J. Kim and Y. Rahmat-Samii, "Implanted antennas inside a human body: Simulations, designs, and characterizations," *IEEE Trans. Microw. Theory Thechn.*, vol. 52, no. 8, pp. 1934–1943, Aug. 2004.

[179] J. T. Chang, M. W. Fanning, P. M. Meaney, and K. D. Paulsen, "A conductive plastic for simulating biological tissue at microwave frequencies," *IEEE Trans. Electromagn. Compat.*, vol. 42, no. 1, pp. 78–81, Feb. 2000.

[180] A. W. Guy, "Analyses of electromagnetic fields induced in biological tissues by thermographic studies on equivalent phantom models," *IEEE Trans. Microw. Theory Techn.*, vol. TMTT-19, no. 2, pp. 205–214, Feb. 1971.

[181] L. E. Maggi, M. A. Krüger, W. C. A. Pereira, and E. E. C. Monteiro, "Development of silicon-based materials for ultrasound biological phantoms," in *Proc. IEEE Int. Ultrason. Symp.*, 2009, pp. 1962–1965.

[182] H. D. Choi, H. W. Shim, K. Y. Cho, H. J. Lee, C. S. Park, and H. G. Yoon, "Electromagnetic and electromagnetic wave-absorbing properties of the $SrTiO_3$-epoxy composite," *J. Appl. Polym. Sci.*, vol. 72, no. 1, pp. 75–83, 1999.

[183] Y. Nikawa, M. Chino, and K. Kikuchi, "Soft and dry phantom modeling material using silicone rubber with carbon fiber," *IEEE Trans. Microw. Theory Techn.*, vol. 44, no. 10, pp. 1949–1953, Oct. 1996.

[184] C. Gabriel, "Tissue equivalent material for hand phantoms," *Phys. Med. Biol.*, vol. 52, no. 14, pp. 4205–4210, 2007.

[185] T. Kobayashi, T. Nojima, K. Yamada, and S. Uebayashi, "Dry phantom composed of ceramics and its application to SAR estimation," *IEEE Trans. Microw. Theory Techn.*, vol. 41, no. 1, pp. 136–140, Jan. 1993.

[186] S. S. Stuchly, "Specific absorption rate distributions in a heterogeneous model of the human body at radiofrequencies," Environ. Prot. Agency, Washington, DC, USA, Rep. EPA/600/1-87/003, 1987, p. 89.

[187] S. S. Stuchly, A. Kraszewski, M. A. Stuchly, G. W. Hartsgrove, and R. J. Spiegel, "RF energy deposition in a heterogeneous model of man: Far-field exposures," *IEEE Trans. Biomed. Eng.*, vol. BME-34, no. 12, pp. 951–957, Dec. 1987.

[188] S. R. H. Davidson and M. D. Sherar, "Measurement of the thermal conductivity of polyacrylamide tissue-equivalent material," *Int. J. Hyperth.*, vol. 19, no. 5, pp. 551–562, 2003.

[189] A. Surowiec, P. N. Shrivastava, M. Astrahan, and Z. Petrovich, "Utilization of a multilayer polyacrylamide phantom for evaluation of hyperthermia applicators," *Int. J. Hyperth.*, vol. 8, no. 6, pp. 795–807, 1992.

[190] K. Ito, K. Furuya, Y. Okano, and L. Hamada, "Development and characteristics of a biological tissue-equivalent phantom for microwaves," *Electron. Commun. Jpn. I*, vol. 84, no. 4, pp. 67–77, 2001.

[191] M. W. Groch, J. A. Urbon, W. D. Erwin, and S. Al-Doohan, "An MRI tissue equivalent lesion phantom using a novel polysaccharide material," *Magn. Reson. Imag.*, vol. 9, no. 3, pp. 417–421, 1991.

[192] K. J. M. Surry, H. J. B. Austin, A. Fenster, and T. M. Peters, "Poly(vinyl alcohol) cryogel phantoms for use in ultrasound and MR imaging," *Phys. Med. Biol.*, vol. 49, pp. 5529–5546, Dec. 2004.
[193] C. Marchal, M. Nadi, A. J. Tosser, C. Roussey, and M. L. Gaulard, "Dielectric properties of gelatine phantoms used for simulations of biological tissues between 10 and 50 MHz," *Int. J. Hyperth.*, vol. 5, no. 6, pp. 725–732, 1989.
[194] T. Sunaga *et al.*, "Development of a dielectric equivalent gel for better impedance matching for human skin," *Bioelectromagnetics*, vol. 24, pp. 725–732, Apr. 2003.
[195] M. Lazebnik, E. L. Madsen, G. R. Frank, and S. C. Hagness, "Tissue-mimicking phantom materials for narrowband and ultrawideband microwave applications," *Phys. Med. Biol.*, vol. 50, pp. 4245–4258, Sep. 2005.
[196] E. L. Madsen, J. A. Zagzebski, and G. R. Frank, "Oil-in-gelatin dispersions for use as ultrasonically tissue-mimicking materials," *Ultrasound Med. Biol.*, vol. 8, no. 3, pp. 277–287, 1982.
[197] A. Tsolis, A. Paraskevopoulos, A. A. Alexandridis, W. G. Whittow, A. Chauraya, and J. C. Vardaxoglou, "Design, realisation and evaluation of a liquid hollow torso phantom appropriate for wearable antenna assessment," *IET Microw. Antennas Propag.*, vol. 11, no. 9, pp. 1308–1316, 2017.
[198] S. Symeonidis, W. G. Whittow, M. Zecca, and C. Panagamuwa, "Bone fracture monitoring using implanted antennas in the radius, tibia and phalange heterogeneous bone phantoms," *Biomed. Phys. Eng. Exp.*, vol. 4, no. 4, pp. 1–10, 2018.
[199] T. Karacolak, R. Cooper, and E. Topsakal, "Electrical properties of rat skin and design of implantable antennas for medical wireless telemetry," *IEEE Trans. Antennas Propag.*, vol. 57, no. 9, pp. 2806–2812, Sep. 2009.
[200] T. Yilmaz, T. Karacolak, and E. Topsakal, "Characterization and testing of a skin mimicking material for implantable antennas operating at ISM band (2.4 GHz-2.48 GHz)," *IEEE Antennas Wireless Propag. Lett.*, vol. 7, pp. 418–420, 2008.
[201] M. Asili, R. Green, S. Seran, and E. Topsakal, "A small implantable antenna for MedRadio and ISM bands," *IEEE Antennas Wireless Propag. Lett.*, vol. 11, pp. 1683–1685, 2012.
[202] E. Topsakal, "Antennas for medical applications: Ongoing research and future challenges," in *Proc. Int. Conf. Electromagn. Adv. Appl.*, 2009, pp. 890–893.
[203] R. B. Green, M. V. Smith, and E. Topsakal, "In vitro and in vivo testing of implantable antennas," in *Antenna and Sensor Technologies in Modern Medical Applications*. Hoboken, NJ, USA: Wiley, 2021, pp. 145–189.
[204] C. K. Chou, G. W. Chen, A. W. Guy, and K. H. Luk, "Formulas for preparing phantom muscle tissue at various radiofrequencies," *Bioelectromagnetics*, vol. 5, no. 4, pp. 435–441, 1984.
[205] H.-Y. Lin, M. Takahashi, K. Saito, and K. Ito, "Performance of implantable folded dipole antenna for in-body wireless communication," *IEEE Trans. Antennas Propag.*, vol. 61, no. 3, pp. 1363–1370, Mar. 2013.
[206] R. Suga, M. Inoue, K. Saito, M. Takahashi, and K. Ito, "Development of multi-layered biological tissue-equivalent phantom for HF band," *IEICE Commun. Exp.*, vol. 2, no. 12, pp. 507–511, 2013.
[207] K. Ito, "Human body phantoms for evaluation of wearable and implantable antennas," in *Proc. Eur. Conf. Antennas Propag.*, 2007, pp. 1–6.
[208] W. G. Whittow, R. M. Edwards, C. J. Panagamuwa, and J. C. Vardaxoglou, "Effect of tongue jewellery and orthodontist metallic braces on the SAR due to mobile phones in different anatomical human head models including children," in *Proc. Loughborough Antennas Propag. Conf.*, 2008, pp. 293–296.
[209] J. Maitra and V. K. Shukla, "Cross-linking in hydrogels—A review," *Amer. J. Polym. Sci.*, vol. 4, no. 2, pp. 25–31, 2014.
[210] I. Chatterjee and O. P. Gandhi, "An inhomogeneous thermal block model of man for the electromagnetic environment," *IEEE Trans. Biomed. Eng.*, vol. BME-30, no. 11, pp. 707–715, Nov. 1983.
[211] I. Chatterjee, M. J. Hagmann, and O. P. Gandhi, "Electromagnetic absorption in a multilayered slab model of tissue under near-field exposure conditions," *Bioelectromagnetics*, vol. 1, no. 4, pp. 379–388, 1980.
[212] M. Zankl and K. Eckerman, "The GSF voxel computational phantom family," in *Handbook of Anatomical Models for Radiation Dosimetry*. Boca Raton, FL, USA. CRC Press, 2010, pp. 65–85.
[213] I. G. Zubal. "Voxelman Phantom Data." [Online]. Available: https://noodle.med.yale.edu/zubal/data.htm (Accessed: Jan. 2, 2022).
[214] I. G. Zubal, C. R. Harrell, E. O. Smith, Z. Rattner, G. Gindi, and P. B. Hoffer, "Computerized three-dimensional segmented human anatomy," *Med. Phys.*, vol. 21, no. 2, pp. 299–302, 1994.
[215] P. J. Dimbylow, "The development of realistic voxel phantoms for electromagnetic field dosimetry," in *Proc. Int. Workshop Nat. Radiol. Prot. Board*, 1995, pp. 1–7.
[216] P. J. Dimbylow, "Electromagnetic field calculations in an anatomically realistic voxel model of the human body," in *Radio Frequency Radiation Dosimetry and Its Relationship to the Biological Effects of Electromagnetic Fields*, B. J. Klauenberg and D. Miklavčič, Eds. Cham, Switzerland: Springer, 2000, pp. 123–131.
[217] P. Dimbylow, "Development of the female voxel phantom, NAOMI, and its application to calculations of induced current densities and electric fields from applied low frequency magnetic and electric fields," *Phys. Med. Biol.*, vol. 50, no. 6, pp. 1047–1070, 2005.
[218] G. Xu. "RPI VIP Man: (RISCC Catalog)." [Online]. Available: https://rsicc.ornl.gov/Catalog.aspx?c=V (Accessed: Jan. 2, 2022).
[219] X. G. Xu and C. Shi, "Preliminary development of a 4D anatomical model for Monte Carlo simulations," in *Proc. Monte Carlo Topical Meeting Monte Carlo Method Versatility Unbounded Dyn. Comput. World*, 2005.
[220] O. P. Gandhi, "Millimeter-resolution MRI-based models of the human body for electromagnetic dosimetry from ELF to microwave frequencies," in *Proc. Int. Workshop Voxel Phantom Develop.*, 1995, pp. 24–31.
[221] A. D. Tinniswood, C. M. Furse, and O. P. Gandhi, "Computations of SAR distributions for two anatomically based models of the human head using CAD files of commercial telephones and the parallelized FDTD code," *IEEE Trans. Antennas Propag.*, vol. 46, no. 6, pp. 829–833, Jun. 1998.
[222] M. J. Ackerman, "Visible human project," *Proc. IEEE*, vol. 86, no. 3, pp. 504–511, Mar. 1998. [Online]. Available: https://www.nlm.nih.gov/research/visible/visible_human.html
[223] K. Saito, K. Sato, S. Kinase, and T. Nagaoka, "Japanese computational phantoms: Otoko, Onago, JM, JM2, JF, TARO, HANAKO, pregnant woman, and deformable child," in *Handbook of Anatomical Models for Radiation Dosimetry*. Boca Raton, FL, USA: CRC Press, 2010, pp. 221–253.
[224] R. Kramer, H. J. Khoury, J. W. Vieira, and V. J. M. Lima, "MAX06 and FAX06: Update of two adult human phantoms for radiation protection dosimetry," *Phys. Med. Biol.*, vol. 51, no. 14, pp. 3331–3346, 2006.
[225] V. F. Cassola, V. J. M. Lima, R. Kramer, and H. J. Khoury, "FASH and MASH: Female and male adult human phantoms based on polygon mesh surfaces: I. Development of the anatomy," *Phys. Med. Biol.*, vol. 55, no. 1, pp. 133–162, 2009.
[226] C. Lee, C. Lee, S.-H. Park, and J.-K. Lee, "Development of the two Korean adult tomographic computational phantoms for organ dosimetry: Two Korean tomographic phantoms," *Med. Phys*, vol. 33, no. 2, pp. 380–390, 2006.
[227] C. Lee and C. H. Kim, "Korean computational phantoms: KMIRD, KORMAN, KORWOMAN, KTMAN-1, KTMAN-2, and HDRK-man," in *Handbook of Anatomical Models for Radiation Dosimetry*. London, U.K.: Chapman Hall, 2009, p. 255.
[228] P. Dimbylow, "Development of pregnant female, hybrid voxel-mathematical models and their application to the dosimetry of applied magnetic and electric fields at 50 Hz," *Phys. Med. Biol.*, vol. 51, no. 10, pp. 2383–2394, 2006.
[229] "OVERVIEW IT'IS Foundation." [Online]. Available: https://itis.swiss/virtual-population/virtual-population/overview/ (Accessed: Jan. 2, 2022).
[230] S. R. Pérez, N. W. Marshall, L. Struelens, and H. Bosmans, "Characterization and validation of the thorax phantom Lungman for dose assessment in chest radiography optimization studies," *J. Med. Img.*, vol. 5, no. 1, 2018, Art. no. 13504.
[231] W. P. Segars, "Development and application of the new dynamic NURBS-based cardiac-torso (NCAT) phantom," Ph.D. dissertation, Dept. Biomed. Eng., Univ. North Carolina, Chapel Hill, NC, USA, 2009.

[232] L. Vancoillie *et al.*, "The creation of a breast cancer voxel model database for virtual clinical trials in digital breast tomosynthesis," in *Proc. Med. Imag. Phys. Med. Imag.*, vol. 11595, Feb. 2021, Art. no. 115950.

[233] E. Zastrow, S. K. Davis, M. Lazebnik, F. Kelcz, B. D. V. Veen, and S. C. Hagness, "Development of anatomically realistic numerical breast phantoms with accurate dielectric properties for modeling microwave interactions with the human breast," *IEEE Trans. Biomed. Eng.*, vol. 55, no. 12, pp. 2792–2800, Dec. 2008.

[234] T. Xie and H. Zaidi, "Development of computational small animal models and their applications in preclinical imaging and therapy research," *Med. Phys.*, vol. 43, no. 1, pp. 111–131, 2016.

[235] D. W. Deno, "Currents induced in the human body by high voltage transmission line electric field measurement and calculation of distribution and dose," *IEEE Trans. Power App. Syst.*, vol. TPAS-96, no. 5, pp. 1517–1527, Sep. 1977.

[236] O. P. Gandhi, G. Lazzi, and C. M. Furse, "Electromagnetic absorption in the human head and neck for mobile telephones at 835 and 1900 MHz," *IEEE Trans. Microw. Theory Techn.*, vol. 44, no. 10, pp. 1884–1897, Oct. 1996.

[237] M. J. Hagmann O. P. Gandhi, J. A. D'Andrea, and I. Chatterjee, "Head resonance: Numerical solutions and experimental results," *IEEE Trans. Microw. Theory Techn.*, vol. TMTT-27, no. 9, pp. 809–813, Sep. 1979.

[238] O. P. Gandhi, "Yes the children are more exposed to radiofrequency energy from mobile telephones than adults," *IEEE Access*, vol. 3, pp. 985–988, 2015.

[239] A. Kiourti and K. S. Nikita, "Numerical assessment of the performance of a scalp-implantable antenna: Effects of head anatomy and dielectric parameters," *Bioelectromagnetics*, vol. 34, no. 3, pp. 167–179, 2013.

[240] F. J. Meyer, D. B. Davidson, U. Jakobus, and M. A. Stuchly, "Human exposure assessment in the near field of GSM base-station antennas using a hybrid finite element/method of moments technique," *IEEE Trans. Biomed. Eng.*, vol. 50, no. 2, pp. 224–233, Feb. 2003.

[241] A. Taflove, A. Oskooi, and S. G. Johnson, *Advances in FDTD Computational Electrodynamics: Photonics and Nanotechnology*. Boston, MA, USA: Artech House, 2013.

[242] R. Hong, K. Chen, X. Hou, Q. Sun, N. Liu, and Q. H. Liu, "Mixed finite element method for full-wave simulation of bioelectromagnetism from DC to microwave frequencies," *IEEE Trans. Biomed. Eng.*, vol. 67, no. 10, pp. 2765–2772, Oct. 2020.

[243] C. M. Furse and O. P. Gandhi, "Calculation of electric fields and currents induced in a millimeter-resolution human model at 60 Hz using the FDTD method," *Bioelectromagnetics*, vol. 19, no. 5, pp. 293–299, 1998.

[244] C. M. Furse, J.-Y. Chen, and O. P. Gandhi, "The use of the frequency-dependent finite-difference time-domain method for induced current and SAR calculations for a heterogeneous model of the human body," *IEEE Trans. Electromagn. Compat.*, vol. 36, no. 2, pp. 128–133, May 1994.

[245] K. Masumnia-Bisheh and C. Furse, "Bioelectromagnetic uncertainty analysis using geometrically stochastic FDFD method," *IEEE Trans. Antennas Propag.*, vol. 69, no. 4, pp. 2433–2436, Apr. 2021.

[246] K. Masumnia-Bisheh, K. Forooraghi, M. Ghaffari-Miab, and C. M. Furse, "Geometrically stochastic FDTD method for uncertainty quantification of EM fields and SAR in biological tissues," *IEEE Trans. Antennas Propag.*, vol. 67, no. 12, pp. 7466–7475, Dec. 2019.

[247] *IEEE Recommended Practice for Measurements and Computations of Electric, Magnetic, and Electromagnetic Fields With Respect to Human Exposure to Such Fields, 0 Hz to 300 GHz*, IEEE Standard C95.3-2021, 2021, pp. 1–240.

[248] *IEEE Standard for Safety Levels With Respect to Human Exposure to Electric, Magnetic, and Electromagnetic Fields, 0 Hz to 300 GHz—Corrigenda 2*, IEEE Standard C95.1-2019/Cor2-2020, 2020, pp. 1–15.

[249] T. Kawamura, K. Saito, S. Kikuchi, M. Takahashi, and K. Ito, "Specific absorption rate measurement of birdcage coil for 3.0-T magnetic resonance imaging system employing thermographic method," *IEEE Trans. Microw. Theory Techn.*, vol. 57, no. 10, pp. 2508–2514, Oct. 2009.

[250] *IEC/IEEE International Standard—Determining the Peak Spatial-Average Specific Absorption Rate (SAR) in the Human Body From Wireless Communications Devices, 30 MHz to 6 GHz—Part 1: General Requirements for Using the Finite-Difference Time-Domain (FDTD) Method for SAR Calculations*, IEC/IEEE Standard 62704-1:2017, 2017, pp. 1–86.

[251] *Determining the Peak Spatial-Average Specific Absorption Rate (SAR) in the Human Body From Wireless Communications Devices, 30 MHz to 6 GHz—Part 3: Specific Requirements for Using the Finite Difference Time Domain (FDTD) Method for SAR Calculations of Mobile Phones*, IEC/IEEE Standard 62704-3:2017, 2017, pp. 1–76.

[252] K. Ito, M. Hyodo, M. Shimura, and H. Kasai, "Thin applicator having coaxial ring slots for interstitial microwave hyperthermia," in *Proc. IEEE Int. Symp. Antennas Propag. Soc.*, 2017, pp. 1233–1236.

[253] A. J. Yu *et al.*, "Ultrasound-guided percutaneous microwave ablation of central intraductal papilloma: A prospective pilot study," *Int. J. Hyperth.*, vol. 36, no. 1, pp. 605–611, 2019.

[254] Z. Li *et al.*, "Image-guided microwave ablation of hepatocellular carcinoma ($\leq$5.0 cm): Is MR guidance more effective than CT guidance?" *BMC Cancer*, vol. 21, no. 1, p. 366, 2021.

[255] A. C. Vorländer *et al.*, "Comparison between microwave ablation and bipolar radiofrequency ablation in benign thyroid nodules: Differences in energy transmission, duration of application and applied shots," *Int. J. Hyperth.*, vol. 35, no. 1, pp. 216–225, 2018.

[256] A. V. Aufranca *et al.*, "Percutaneous thermal ablation of primary and secondary lung tumors: Comparison between microwave and radiofrequency ablation," *Diagn. Interv. Imag.*, vol. 100, no. 12, pp. 781–791, 2019.

[257] A. E. Schena, P. Saccomandi, and Y. Fong, "Laser ablation for cancer: Past, present and future," *J. Funct. Biomater.*, vol. 8, no. 2, p. 19, 2017.

[258] B. T. McWilliams, E. E. Schnell, S. Curto, T. M. Fahrbach, and P. Prakash, "A directional interstitial antenna for microwave tissue ablation: Theoretical and experimental investigation," *IEEE Trans. Biomed. Eng.*, vol. 62, no. 9, pp. 2144–2150, Sep. 2015.

[259] A. Y. Mohtashami, S. C. Hagness, and N. Behdad, "A hybrid slot/monopole antenna with directional heating patterns for microwave ablation," *IEEE Trans. Antennas Propag.*, vol. 65, no. 8, pp. 3889–3896, Aug. 2017.

[260] A. J. Sebek, S. Curto, and J. Eaton-Evans, "Feasibility assessment of microwave ablation for treating esophageal varices," *J. Med. Devices*, vol. 11, no. 3, p. 8, 2017.

[261] A. H. Luyen, S. C. Hagness, and N. Behdad, "A minimally invasive coax-fed microwave ablation antenna with a tapered balun," *IEEE Trans. Antennas Propag.*, vol. 65, no. 12, pp. 7280–7287, Dec. 2017.

[262] A. Y. Endo, K. Saito, and K. Ito, "The development of forceps-type microwave tissue coagulator for surgical operation," *IEEE Trans. Microw. Theory Techn.*, vol. 63, no. 6, pp. 2041–2049, Jun. 2015.

[263] A. T. Tani, S. Naka, and S. Tani, "The invention of microwave surgical scissors for seamless coagulation and cutting," *Surg. Today*, vol. 48, pp. 856–864, Sep. 2018.

[264] A. J. Chiang, S. Birla, M. Bedoya, D. Jones, J. Subbiah, and C. L. Brace, "Modeling and validation of microwave ablations with internal vaporization," *IEEE Trans. Biomed. Eng.*, vol. 62, no. 2, pp. 657–663, Feb. 2015.

[265] A. Y. Endo, K. Saito, and K. Ito, "Temperature analysis of liver tissue in microwave coagulation therapy considering tissue dehydration by heating," *IEICE Trans. Electron.*, vol. E99.C, no. 2, pp. 257–265, 2016.

[266] A. C. Reimann *et al.*, "Planar microwave sensor for theranostic therapy of organic tissue based on oval split ring resonators," *Sensors*, vol. 16, no. 9, pp. 1450–1462, 2016.

[267] J. H. Larsen and L. E. Jacobi, *Medical Applications of Microwave Imaging*. New York, NY, USA: IEEE Press, 1985.

[268] J.-C. Bolomey, "Advancing microwave-based imaging techniques for medical applications in the wake of the 5G revolution," in *Proc. 13th Eur. Conf. Antennas Propag.*, 2019, pp. 1–5.

[269] N. K. Nikolova, *Introduction to Microwave Imaging*. Cambridge, U.K.: Cambridge Univ. Press, 2017.

[270] X. Chen, *Computational Methods for Electromagnetic Inverse Scattering*. Hoboken, NJ, USA: Wiley, 2018.

[271] M. Pastorino and A. Randazzo, *Microwave Imaging Methods and Applications*. Boston, MA, USA: Artech House, 2018.

[272] D. O'Loughlin, M. O'Halloran, B. M. Moloney, M. Glavin, E. Jones, and M. A. Elahi, "Microwave breast imaging: Clinical advances and remaining challenges," *IEEE Trans. Biomed. Eng.*, vol. 65, no. 11, pp. 2580–2590, Nov. 2018.

[273] P. M. Meaney, "Microwave imaging for neoadjuvant chemotherapy monitoring: Initial clinical experience," *Breast Cancer Res.*, vol. 15, no. 2, p. R35, 2013.

[274] M. Shere, I. Lyburn, R. Sidebottom, H. Massey, C. Gillett, and L. Jones, "MARIA®M5: A multicentre clinical study to evaluate the ability of the Micrima radio-wave radar breast imaging system (MARIA®) to detect lesions in the symptomatic breast," *Eur. J. Radiol.*, vol. 116, pp. 61–67, Jul. 2019.

[275] A. Fasoula, "Pilot patient study with the Wavelia Microwave Breast Imaging system for breast cancer detection: Clinical feasibility and identified technical challenges," in *Proc. 14th Eur. Conf. Antennas Propag. (EuCAP)*, 2020, pp. 1–5.

[276] B. R. Lavoie, M. Okoniewski, and E. C. Fear, "Estimating the effective permittivity for reconstructing accurate microwave-radar images," *PLoS One*, vol. 11, no. 9, 2016, Art. no. 160849.

[277] A. Fhager, S. Candefjord, M. Elam, and M. Persson, "Microwave diagnostics ahead: Saving time and the lives of trauma and stroke patients," *IEEE Microw. Mag.*, vol. 19, no. 3, pp. 78–90, May 2018.

[278] A. Fedeli, V. Schenone, A. Randazzo, M. Pastorino, T. Henriksson, and S. Semenov, "Nonlinear S-parameters inversion for stroke imaging," *IEEE Trans. Microw. Theory Techn.*, vol. 69, no. 3, pp. 1760–1771, Mar. 2021.

[279] P.-H. Tournier, "Numerical modeling and high-speed parallel computing: New perspectives on tomographic microwave imaging for brain stroke detection and monitoring," *IEEE Antennas Propag. Mag.*, vol. 59, no. 5, pp. 98–110, Oct. 2017.

[280] A. S. M. Alqadami, A. Trakic, A. E. Stancombe, B. Mohammed, K. Bialkowski, and A. Abbosh, "Flexible electromagnetic cap for head imaging," *IEEE Trans. Biomed. Circuits Syst.*, vol. 14, no. 5, pp. 1097–1107, Oct. 2020.

[281] "EMTensor." [Online]. Available: https://www.emtensor.com/ (Accessed: Jan. 2, 2022).

[282] "EMVision Reports Very Encouraging Pilot Clinical Trial Data." 2020. [Online]. Available: https://www.listcorp.com/asx/emv/emvision-medical-devices-limited/news/emvision-reports-very-encouraging-pilot-clinical-trial-data-2390126.html

[283] P. M. Meaney *et al.*, "Clinical microwave tomographic imaging of the calcaneus: A first-in-human case study of two subjects," *IEEE Trans. Biomed. Eng.*, vol. 59, no. 12, pp. 3304–3313, Dec. 2012.

[284] A. Darvazehban, S. A. Rezaeieh, A. Zamani, and A. M. Abbosh, "Pattern reconfigurable metasurface antenna for electromagnetic torso imaging," *IEEE Trans. Antennas Propag.*, vol. 67, no. 8, pp. 5453–5462, Aug. 2019, doi: 10.1109/TAP.2019.2916576.

[285] K. S. Sultan, B. Mohamed, M. Manoufali, and A. Abbosh, "Portable electromagnetic knee imaging system," *IEEE Trans. Antennas Propag.*, vol. 69, no. 10, pp. 6824–6837, Oct. 2021.

[286] K. Sultan, A. Mahmoud, and A. M. Abbosh, "Textile electromagnetic brace for knee imaging," *IEEE Trans. Biomed. Circuits Syst.*, vol. 15, no. 3, pp. 522–536, Jun. 2021.

[287] C. Dachena, A. Fedeli, A. Fanti, M. B. Lodi, M. Pastorino, and A. Randazzo, "Microwave imaging for the diagnosis of cervical diseases: A feasibility analysis," *IEEE J. Electromagn., RF, Microw. Med. Biol.*, vol. 5, no. 3, pp. 277–285, Sep. 2021.

[288] A. T. Mobashsher and A. M. Abbosh, "Artificial human phantoms: Human proxy in testing microwave apparatuses that have electromagnetic interaction with the human body," *IEEE Microw. Mag.*, vol. 16, no. 6, pp. 42–62, Jul. 2015.

[289] M. J. During *et al.*, "Controlled release of dopamine from a polymeric brain implant: In vivo characterization," *Ann. Neurol.*, vol. 25, no. 4, pp. 351–356, 1989.

[290] V. S. Polikov, P. A. Tresco, and W. M. Reichert, "Response of brain tissue to chronically implanted neural electrodes," *J. Neurosci. Methods*, vol. 148, pp. 1–18, Oct. 2005.

[291] K. D. Wise, A. M. Sodagar, Y. Yao, M. N. Gulari, G. E. Perlin, and K. Najafi, "Microelectrodes, microelectronics, and implantable neural microsystems," *Proc. IEEE*, vol. 96, no. 7, pp. 1184–1202, Jul. 2008.

[292] A. Waziri, "Initial surgical experience with a dense cortical microarray in epileptic patients undergoing craniotomy for subdural electrode implantation," *Neurosurgery*, vol. 64, no. 3, pp. 540–545, 2009.

[293] J. Dethier, P. Nuyujukian, S. I. Ryu, K. Shenoy, and K. Boahen, "Design and validation of a real-time spiking-neural-network decoder for brain-machine interfaces," *J. Neural Eng.*, vol. 10, no. 3, 2013, Art. no. 36008.

[294] S. Kim, P. Tathireddy, R. A. Normann, and F. Solzbacher, "Thermal impact of an active 3-D microelectrode array implanted in the brain," *IEEE Trans. Neural Syst. Rehabil. Eng.*, vol. 15, no. 4, pp. 493–501, Dec. 2007.

[295] T. Bjorninen *et al.*, "Design of wireless links to implanted brain–machine interface microelectronic systems," *IEEE Antennas Wireless Propag. Lett.*, vol. 11, pp. 1663–1666, 2012.

[296] M. Mark, T. Björninen, L. Ukkonen, L. Sydänheimo, and J. M. Rabaey, "SAR reduction and link optimization for mm-size remotely powered wireless implants using segmented loop antennas," in *Proc. IEEE Topical Conf. Biomed. Wireless Technol. Netw. Sens. Syst.*, 2011, pp. 7–10.

[297] E. Moradi, T. Björninen, L. Sydänheimo, J. M. Carmena, J. M. Rabaey, and L. Ukkonen, "Measurement of wireless link for brain–machine interface systems using human-head equivalent liquid," *IEEE Antennas Wireless Propag. Lett.*, vol. 12, pp. 1307–1310, 2013.

[298] M. W. A. Khan, T. Björninen, L. Sydänheimo, and L. Ukkonen, "Characterization of two-turns external loop antenna with magnetic core for efficient wireless powering of cortical implants," *IEEE Antennas Wireless Propag. Lett.*, vol. 15, pp. 1410–1413, 2016.

[299] K. Guido and A. Kiourti, "Passive RF neural electrodes," in *Neural Interface Engineering: Linking the Physical World and the Nervous System*, vol. 12. Dordrecht, The Netherlands: Springer, 2020, pp. 299–319.

[300] A. Abbaspour-Tamijani, M. F. Farooqui, B. C. Towe, and J. Chae, "A miniature fully-passive microwave back-scattering device for short-range telemetry of neural potentials," in *Proc. 30th Annu. Int. Conf. IEEE Eng. Med. Biol. Soc.*, 2008, pp. 129–132.

[301] H. N. Schwerdt, "A fully passive wireless microsystem for recording of neuropotentials using RF backscattering methods," *J. Microelectromech. Syst.*, vol. 20, no. 5, pp. 1119–1130, Oct. 2011.

[302] H. N. Schwerdt, F. A. Miranda, and J. Chae, "Analysis of electromagnetic fields induced in operation of a wireless fully passive backscattering neurorecording microsystem in emulated human head tissue," *IEEE Trans. Microw. Theory Techn.*, vol. 61, no. 5, pp. 2170–2176, May 2013.

[303] C. W. L. Lee, A. Kiourti, J. Chae, and J. L. Volakis, "A high-sensitivity fully passive neurosensing system for wireless brain signal monitoring," *IEEE Trans. Microw. Theory Techn.*, vol. 63, no. 6, pp. 2060–2068, Jun. 2015.

[304] A. Kiourti, C. W. L. Lee, J. Chae, and J. L. Volakis, "A wireless fully passive neural recording device for unobtrusive neuropotential monitoring," *IEEE Trans. Biomed. Eng.*, vol. 63, no. 1, pp. 131–137, Jan. 2016.

[305] C. W. L. Lee, A. Kiourti, and J. L. Volakis, "Miniaturized fully passive brain implant for wireless neuropotential acquisition," *IEEE Antennas Wireless Propag. Lett.*, vol. 16, pp. 645–648, 2017.

[306] K. Guido and A. Kiourti, "An in vivo-mimicking in vitro testbed for brain-computer interfaces," *IEEE J. Electromagn., RF, Microw. Med. Biol.*, vol. 4, no. 4, pp. 240–246, Dec. 2020.

[307] H. N. Schwerdt, F. A. Miranda, and J. Chae, "Wireless fully passive multichannel recording of neuropotentials using photo-activated RF backscattering methods," *IEEE Trans. Microw. Theory Techn.*, vol. 63, no. 9, pp. 2965–2970, Sep. 2015.

[308] W.-C. Chen, C. W. L. Lee, A. Kiourti, and J. L. Volakis, "A multi-channel passive brain implant for wireless neuropotential monitoring," *IEEE J. Electromagn., RF, Microw. Med. Biol.*, vol. 2, no. 4, pp. 262–269, Dec. 2018.

[309] K. Guido and A. Kiourti, "Real world considerations for wireless and batteryless brain implants," in *Proc. Int. Workshop Antenna Technol.*, Miami, FL, USA, Mar. 2019, pp. 3–6.

[310] W. M. Grill, S. E. Norman, and R. V. Bellamkonda, "Implanted neural interfaces: Biochallenges and engineered solutions," *Annu. Rev. Biomed. Eng.*, vol. 11, pp. 1–24, Jul. 2009.

[311] B. He *et al.*, "Grand challenges in interfacing engineering with life sciences and medicine," *IEEE Trans. Biomed. Eng.*, vol. 60, no. 3, pp. 589–598, Mar. 2013.
[312] M. Machnoor and G. Lazzi, "High-efficiency multicoil wireless power and data transfer for biomedical implants and neuroprosthetics," in *Antenna and Sensor Technologies in Modern Medical Applications*. Hoboken, NJ, USA: Wiley, 2021, ch. 8.
[313] A. K. RamRakhyani and G. Lazzi, "Power/data telemetry techniques for implants or wearable systems," in *Electromagnetics of Body Area Networks: Antennas, Propagation*. Piscataway, NJ, USA: Wiley, 2016, ch. 14.
[314] M. Ghovanloo and G. Lazzi, "Transcutaneous magnetic coupling of power and data," in *Encyclopedia of Biomedical Engineering*. Hoboken, NJ, USA: Wiley, 2006.
[315] J. Paknahad, K. Loizos, L. Yu, M. S. Humayun, and G. Lazzi, "Color and cellular selectivity of retinal ganglion cell subtypes through frequency modulation of electrical stimulation," *Sci. Rep.*, vol. 11, no. 1, p. 5177, 2021.
[316] P. Kosta *et al.*, "Model-based comparison of current flow in rod bipolar cells of healthy and early-stage degenerated retina," *Exp. Eye Res.*, vol. 207, Jun. 2021, Art. no. 108554.
[317] J. Paknahad, K. Loizos, M. Humayun, and G. Lazzi, "Targeted stimulation of retinal ganglion cells in epiretinal prostheses: A multiscale computational study," *IEEE Trans. Neural Syst. Rehabil. Eng.*, vol. 28, no. 11, pp. 2548–2556, Nov. 2020.
[318] C. S. Bingham *et al.*, "Admittance method for estimating local field potentials generated in a multi-scale neuron model of the hippocampus," *Front. Comput. Neurosci.*, vol. 14, p. 72, Aug. 2020.
[319] D. Brizi, J. P. Stang, A. Monorchio, and G. Lazzi, "A compact magnetically dispersive surface for low-frequency wireless power transfer applications," *IEEE Trans. Antennas Propag.*, vol. 68, no. 3, pp. 1887–1895, Mar. 2020.
[320] M. Machnoor, E. S. G. Rodríguez, P. Kosta, J. Stang, and G. Lazzi, "Analysis and design of a 3-coil wireless power transmission system for biomedical applications," *IEEE Trans. Antennas Propag.*, vol. 67, no. 8, pp. 5012–5024, Aug. 2019.
[321] E. S. G. Rodríguez, M. Machnoor, and G. Lazzi, "On the generation of nondiffracting beams in extremely subwavelength applications," *IEEE Trans. Antennas Propag.*, vol. 65, no. 10, pp. 5228–5237, Oct. 2017.
[322] E. S. G. Rodríguez, A. K. RamRakhyani, D. Schurig, and G. Lazzi, "Compact low-frequency metamaterial design for wireless power transfer efficiency enhancement," *IEEE Trans. Microw. Theory Techn.*, vol. 64, no. 5, pp. 1644–1654, May 2016.
[323] A. Rajagopalan, A. RamRakhyani, D. Schurig, and G. Lazzi, "Improving power transfer efficiency of a short-range telemetry system using compact metamaterials," *IEEE Trans. Microw. Theory Techn.*, vol. 62, no. 4, pp. 947–955, Apr. 2014.
[324] E. Margalit *et al.*, "Retinal prosthesis for the blind," *Surv. Ophthalmol.*, vol. 47, no. 4, pp. 335–356, 2002.
[325] K. Gosalia, M. S. Humayun, and G. Lazzi, "Impedance matching and implementation of planar space-filling dipoles as intraocular implanted antennas in a retinal prosthesis," *IEEE Trans. Antennas Propag.*, vol. 53, no. 8, pp. 2365–2373, Aug. 2005.
[326] N. Papadopoulos, N. Melanitis, A. Lozano, C. Soto-Sanchez, E. Fernandez, and K. S. Nikita, "Machine learning method for functional assessment of retinal models," in *Proc. 43rd Annu. Int. Conf. IEEE Eng. Med. Biol. Soc. (EMBC)*, 2021, pp. 4293–4296.
[327] N. Papadopoulos, N. Melanitis, A. Lozano, C. Soto-Sanchez, E. Fernandez, and K. S. Nikita, "Assessing vision quality in retinal prosthesis implantees through deep learning: Current progress and improvements by optimizing hardware design parameters and rehabilitation," in *Proc. 43rd Annu. Int. Conf. IEEE Eng. Med. Biol. Soc. (EMBC)*, 2021, pp. 6130–6133.